South Dakota State University

Open PRAIRIE: Open Public Research Access Institutional Repository and Information Exchange

Electronic Theses and Dissertations

2018

Simulation of Different Rib Shapes in Square Channel

Md Sahedul Islam
South Dakota State University

Follow this and additional works at: https://openprairie.sdstate.edu/etd

Part of the Mechanical Engineering Commons

Recommended Citation

Islam, Md Sahedul, "Simulation of Different Rib Shapes in Square Channel" (2018). *Electronic Theses and Dissertations*. 2679.
https://openprairie.sdstate.edu/etd/2679

This Thesis - Open Access is brought to you for free and open access by Open PRAIRIE: Open Public Research Access Institutional Repository and Information Exchange. It has been accepted for inclusion in Electronic Theses and Dissertations by an authorized administrator of Open PRAIRIE: Open Public Research Access Institutional Repository and Information Exchange. For more information, please contact michael.biondo@sdstate.edu.

SIMULATION OF DIFFERENT RIB SHAPES IN SQUARE CHANNEL

BY

MD SAHEDUL ISLAM

A thesis submitted in partial fulfillment of the requirements for the

Master of Science

Major in Mechanical Engineering

South Dakota State University

2018

SIMULATION OF DIFFERENT RIB SHAPES IN SQUARE CHANNEL

MD SAHEDUL ISLAM

This thesis is approved as a creditable and independent investigation by a candidate for the Master of Science in Mechanical Engineering degree and is acceptable for meeting all the thesis requirements for this degree. Acceptance of this does not imply that the conclusions reached by the candidates are necessarily the conclusions of the major department.

Jeffrey Doom, Ph.D. Date
Thesis Advisor

Kurt Bassett, Ph.D. Date
Head, Department of Mechanical Engineering

Dean, Graduate School Date

ACKNOWLEDGEMENTS

My sincere gratitude goes first to my advisor Dr. Jeffrey Doom for his understanding, wisdom, patience, enthusiasm, and encouragement and for pushing me farther than I could go. I would also like to thank the faculty and staff at the Department of Mechanical Engineering for their help and guidance. To my committee, Dr. Jeffrey Doom, Dr. Huitian Lu and Dr. David Reynolds I am extremely grateful for your assistance and invaluable input for my project. Most of all, I am fully indebted to my family and friends for always being there for me.

TABLE OF CONTENTS

ABBREVIATIONS vi

LIST OF FIGURES vii

ABSTRACT xii

CHAPTER 1: INTRODUCTION 1

1.1 External Cooling Method 2
1.2 Internal Cooling Method 2
1.2.1 Jet Impingement Cooling 3
1.2.2 Rib-Turbulated Cooling 4
1.2.3 Pin-Fin Cooling 4
1.3 Effect of Rib-Turbulator in Coolant Flow 4

CHAPTER 2: LITERATURE REVIEW 6

2.1 Previous Research 6
2.2 Key findings from Previous Research 9
2.3 Research Contribution and Objective 10

CHAPTER 3: METHOD AND APPROACH 11

3.1 CAD Model Generation 11
3.2 Discretization 14
3.3 Fluid Modeling 15
3.4 Governing Equations 16
3.5 Validation Case 17

CHAPTER 4: RESULT AND DISCUSSION 19

4.1 Validation Case Results 19
4.2 Square Rib Results 23
4.2.1 Transverse Square Rib Results 23
4.2.2 45° Square Rib Results 25
4.3 Isosceles Triangular Rib Results 27
4.3.1 Transverse Isosceles Triangular Rib Results 27

4.3.2 45° Isosceles Triangular Rib Results 29
4.4 Pentagon Rib Results 31
4.4.1 Transverse Pentagon Rib Results 31
4.4.2 45° Pentagon Rib Results 33
4.5 Right Triangular Rib Pointing Downstream Results 35
4.5.1 Transverse Right Triangular Rib Pointing Downstream Results 35
4.5.2 45° Right Triangular Rib Pointing Downstream Results 37
4.6 Right Triangular Rib Pointing Upstream Results 39
4.6.1 Transverse Right Triangular Rib Pointing Upstream Results 39
4.6.2 45° Right Triangular Rib Pointing Upstream Results 41
4.7 Pie-Slice Rib Pointing Downstream Results 43
4.7.1 Transverse Pie-Slice Rib Pointing Downstream Results 43
4.7.2 45° Pie-Slice Rib Pointing Downstream Results 45
4.8 Pie-Slice Rib Pointing Upstream Results 47
4.8.1 Transverse Pie-Slice Rib Pointing Upstream Results 47
4.8.2 45° Pie-Slice Rib Pointing Upstream Results 49
4.9 Rectangular Rib Results 51
4.9.1 Transverse Rectangular Rib Results 51
4.9.2 45° Rectangular Rib Results 53
4.10 Comparison of Transverse Ribs 55
4.11 Comparison of 45° Ribs 56
4.12 Comparison of Transverse and 45° Ribs 57
CHAPTER 5: CONCLUSION 59
CHAPTER 6: FUTURE WORK 60
APPENDIX 61
REFERENCES 65

ABBREVIATIONS

A = Area (m^2)

α = Angle of attack (°)

e = Rib height (m)

H = Channel height (m)

w_r = Rib width (m)

W = Channel width (m)

S = Distance between two adjacent ribs or pitch (m)

CAD = Computer-aided design

CFD = Computational fluid dynamics

AR = Aspect ratio (ratio of width to height)

K_H = Kinetic energy

P_{in} = Inlet pressure (Pa)

P_{out} = Outlet pressure (Pa)

ΔP = Pressure drop (Pa)

Re = Reynolds number

ρ = Density (kg/m^3)

v = Velocity (m/s)

D_h = Hydraulic diameter (m)

μ = Dynamic viscosity ($kgm^{-1}s^{-1}$)

WVGs = Winglet vortex generators

∇ = Gradient operator

LIST OF FIGURES

Figure 1.1. Schematic of film-cooling concept [3]. 2

Figure 1.2. Cooling concepts of a modern multipass turbine blade [5]. 3

Figure 1.3. Schematic of flow separation and rib orientations in heat-transfer coefficient enhancement [8]. 4

Figure 3.1. The base of model 11

Figure 3.2. Three-dimensional representation by extruding 12

Figure 3.3. Transparent view of model with outline of ribs 13

Figure 3.4. Transparent view of 3D CAD model with square ribs 14

Figure 3.5. Geometry specifications of validation case [26] 17

Figure 4.1. Two-pass square channel with 45° square ribs CAD model for validation ... 20

Figure 4.2. Nusselt number contour plot for two-pass rib-roughened square channel 20

Figure 4.3. Absolute pressure contour plot for two-pass rib-roughened square channel . 21

Figure 4.4. Temperature contour plot for two-pass rib-roughened square channel 21

Figure 4.5. Average Nusselt number in square rib-roughened channel with different angles 22

Figure 4.6. CAD model of transverse square ribs 23

Figure 4.7. Nusselt number contour plot for transverse square rib 23

Figure 4.8. Absolute pressure contour plot for transverse square rib 24

Figure 4.9. Temperature contour plot for transverse square rib 24

Figure 4.10. CAD model of 45° square ribs 25

Figure 4.11. Nusselt number contour plot for 45° square rib 25

Figure 4.12. Absolute pressure contour plot for 45° square rib 26

Figure 4.13. Temperature contour plot for 45° square ribs 26

Figure 4.14. CAD model of transverse isosceles triangular ribs 27

Figure 4.15. Nusselt number contour plot for transverse isosceles triangular rib 27

Figure 4.16. Absolute pressure contour plot for transverse isosceles triangular rib 28

Figure 4.17. Temperature contour plot for transverse isosceles triangular rib 28

Figure 4.18. CAD model of 45° isosceles triangular ribs 29

Figure 4.19. Nusselt number contour plot for 45° isosceles triangular rib 29

Figure 4.20. Absolute pressure contour plot for 45° isosceles triangular rib 30

Figure 4.21. Temperature contour plot for 45° isosceles triangular rib 30

Figure 4.22. CAD model of transverse pentagon ribs 31

Figure 4.23. Nusselt number contour plot for transverse pentagon rib 31

Figure 4.24. Absolute Pressure contour plot for transverse pentagon rib 32

Figure 4.25. Temperature contour plot for transverse pentagon rib 32

Figure 4.26. CAD model of 45° pentagon ribs 33

Figure 4.27. Nusselt number contour plot for 45° pentagon rib 33

Figure 4.28. Absolute Pressure contour plot for 45° pentagon rib 34

Figure 4.29. Temperature contour plot for 45° pentagon rib 34

Figure 4.30. CAD model of transverse right triangular rib pointing downstream 35

Figure 4.31. Nusselt number contour plot for transverse right triangular rib pointing downstream 35

Figure 4.32. Absolute Pressure contour plot for transverse right triangular rib pointing downstream 36

Figure 4.33. Temperature contour plot for transverse right triangular rib pointing downstream 36
Figure 4.34. CAD model of 45° right triangular rib pointing downstream 37
Figure 4.35. Nusselt number contour plot for 45° right triangular rib pointing downstream 37
Figure 4.36. Absolute Pressure contour plot for 45° right triangular rib pointing downstream 38
Figure 4.37. Temperature contour plot for 45° right triangular rib pointing downstream 38
Figure 4.38. CAD model of transverse right triangular rib pointing upstream..... 39
Figure 4.39. Nusselt number contour plot for transverse right triangular rib pointing upstream 39
Figure 4.40. Absolute Pressure contour plot for transverse right triangular rib pointing upstream 40
Figure 4.41. Temperature contour plot for transverse right triangular rib pointing upstream 40
Figure 4.42. CAD model of 45° right triangular rib pointing upstream 41
Figure 4.43. Nusselt number contour plot for 45° right triangular rib pointing upstream 41
Figure 4.44. Absolute Pressure contour plot for 45° right triangular rib pointing upstream 42
Figure 4.45. Temperature contour plot for 45° right triangular rib pointing upstream 42
Figure 4.46. CAD model of transverse pie-slice rib pointing downstream 43
Figure 4.47. Nusselt number contour plot for transverse pie-slice rib pointing downstream 43

Figure 4.48. Absolute Pressure contour plot for transverse pie-slice rib pointing downstream 44

Figure 4.49. Temperature contour plot for transverse pie-slice rib pointing downstream 44

Figure 4.50. CAD model of 45° pie-slice rib pointing downstream 45

Figure 4.51. Nusselt number contour plot for 45° pie-slice rib pointing downstream 45

Figure 4.52. Absolute Pressure contour plot for 45° pie-slice rib pointing downstream . 46

Figure 4.53. Temperature contour plot for 45° pie-slice rib pointing downstream 46

Figure 4.54. CAD model of transverse pie-slice rib pointing upstream 47

Figure 4.55. Nusselt number contour plot for transverse pie-slice rib pointing upstream 47

Figure 4.56. Absolute Pressure contour plot for transverse pie-slice rib pointing upstream 48

Figure 4.57. Temperature contour plot for transverse pie-slice rib pointing upstream ... 48

Figure 4.58. CAD model of 45° pie-slice rib pointing upstream 49

Figure 4.59. Nusselt number contour plot for 45° pie-slice rib pointing upstream 49

Figure 4.60. Absolute Pressure contour plot for 45° pie-slice rib pointing upstream 50

Figure 4.61. Temperature contour plot for 45° pie-slice rib pointing upstream 50

Figure 4.62. CAD model of transverse rectangular rib 51

Figure 4.63. Nusselt number contour plot for transverse rectangular rib 51

Figure 4.64. Absolute Pressure contour plot for transverse rectangular rib 52

Figure 4.65. Temperature contour plot for transverse rectangular rib 52

Figure 4.66. CAD model of 45° rectangular rib 53

Figure 4.67. Nusselt number contour plot for 45° rectangular rib 53

Figure 4.68. Absolute Pressure contour plot for 45° rectangular rib 54

Figure 4.69. Temperature contour plot for 45° rectangular rib 54

Figure 4.70. Average Nusselt number of rib-roughened surface of different rib shapes (transverse) 55

Figure 4.71. Pressure drop between inlet and outlet of square channel of different rib shapes (transverse) 55

Figure 4.72. Average Nusselt number of rib-roughened surface of different rib shapes (45°) 56

Figure 4.73. Pressure drop between inlet and outlet of square channel of different rib shapes (45°) 56

Figure 4.74. Average Nusselt number of the rib-roughened surface of transverse and 45° ribs 57

Figure 4.75. Pressure drop between inlet and outlet of square channel of transverse and 45° ribs 58

ABSTRACT

SIMULATION OF DIFFERENT RIB SHAPES IN SQUARE CHANNEL

MD SAHEDUL ISLAM

2018

This study investigates heat transfer and pressure drop for rib-roughened square channel without bleed. To optimize the shape of rib, CFD tools were used to model and simulate channel flow with a variety of rib angles and geometries. To validate simulations and determine the turbulence model, experimental results for two-pass channels with ribs at 45˚ angles with BR = 0 and Re = 25,000 was compared. It was found after conducting simulations with different turbulence models that SST turbulence model gave the best results.

CHAPTER 1: INTRODUCTION

Gas turbine is a multifaceted power source which has a growing number of applications such as, aircraft propulsion, industrial or land-based power generation. The development of gas turbine depended on the preexisting development of many devices including windmill, steam turbines etc. Particularly, the development of efficient compressors and materials that can withstand the high temperatures required to operate gas turbine.

The operating temperature of modern gas turbines operate is very high [1] and it is about 2500°F to 2600°F. And by increasing the temperature of the rotor inlet temperature (RIT) of gas turbines, thermal efficiency and power output can also be increased. With the increase in RIT, turbine blade temperature increases. The operating temperatures exceed the material allowable temperature. So, for safe operation the blades in gas turbine must be cooled.

To cool the turbine blade intensively, various cooling methods were developed over the last several decades. Turbine blades are cooled externally and internally. External cooling is also known as film cooling. Internal cooling includes jet impingement cooling, pin-fin cooling and rib-turbulated cooling.

Typically cooling is achieved by using the extracted cool air from the compressor. Because work has been done to compress the air, it effects the overall system efficiency. And also introducing cool air into the mainstream flow imposes further thermodynamic penalties. So, it is important to maximize heat transfer while minimizing the air flow from compressor to accomplish efficient cooling.

1.1 External Cooling Method

Film cooling or external cooling can be achieved by injecting coolant at one or more discrete locations along surface exposed to a high temperature [2]. It protects turbine blade surface directly from the hot gases. Discrete hole film cooling is used to cool turbine airfoil surfaces, shrouds, blade tips [1].

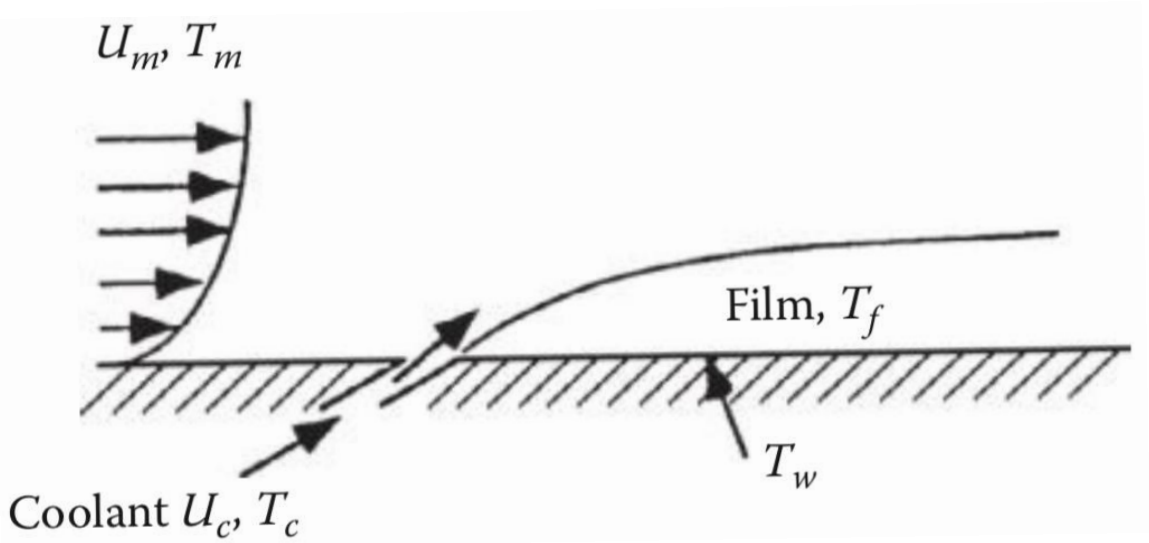

Figure 1.1. Schematic of film-cooling concept [3]

1.2 Internal Cooling Method

The concept of internal cooling of turbine is as old as the turbojet engine itself.

The first production turbojet engine used internal cooling [4]. Typically, jet impingement cooling is used in leading edge, rib-turbulated cooling is used in the mid-chord region and pin-fin cooling is used in trailing edge of the turbine blades.

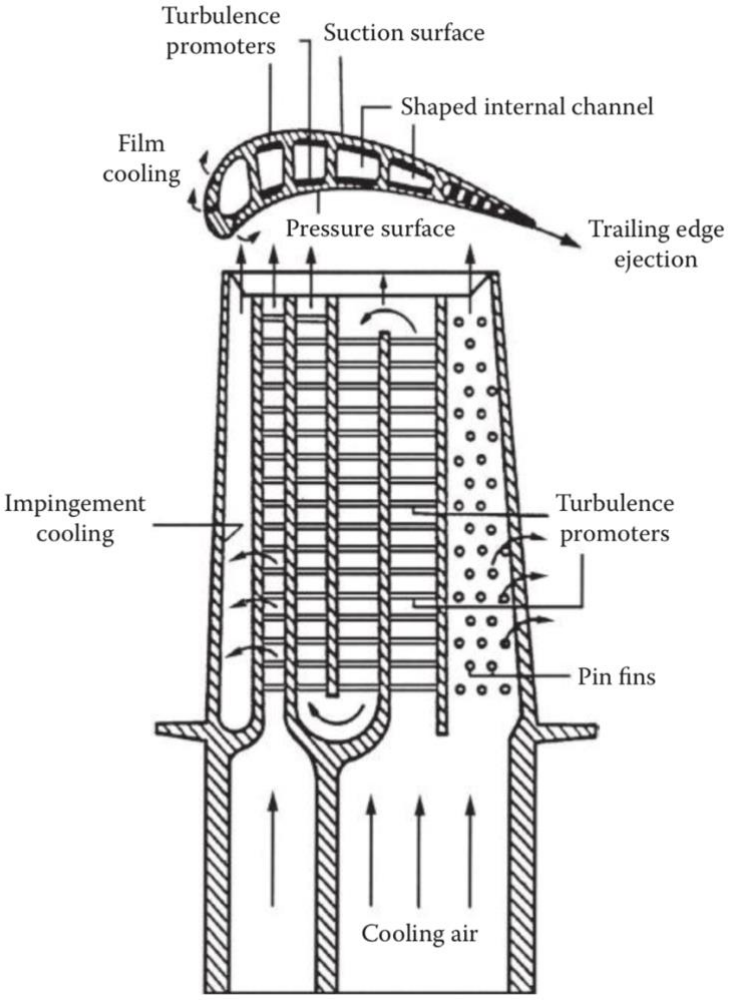

Figure 1.2. Cooling concepts of a modern multipass turbine blade [5]

1.2.1 Jet Impingement Cooling

Jet impingement cooling method can only be used in the leading edge because of space constraints. Thicker cross section and highest thermal load make it the most suitable for leading edge. This method has better heat transfer coefficient compared to other internal cooling method [6].

1.2.2 Rib-Turbulated Cooling

Most of the turbine blades have rib-turbulated serpentine internal cooling channels to enhance heat transfer [7]. Turbulators or ribs are used in two opposite walls in advanced gas turbine blades. For experimental studies, ribs used are square, blockage ratio is from 0.05 to 0.2 and pitch-to-height ratio is from 7 to 15 generally [1].

1.2.3 Pin-Fin Cooling

In this method, circular pins protruding from the heat transfer surface are used.

The pins are oriented perpendicular to the direction of coolant flow to get the maximum convective heat transfer [1]. This method is mainly used in narrow trailing edge of the turbine blades because impingement cooling and rib-turbulated cooling is not possible due to manufacturing constraint.

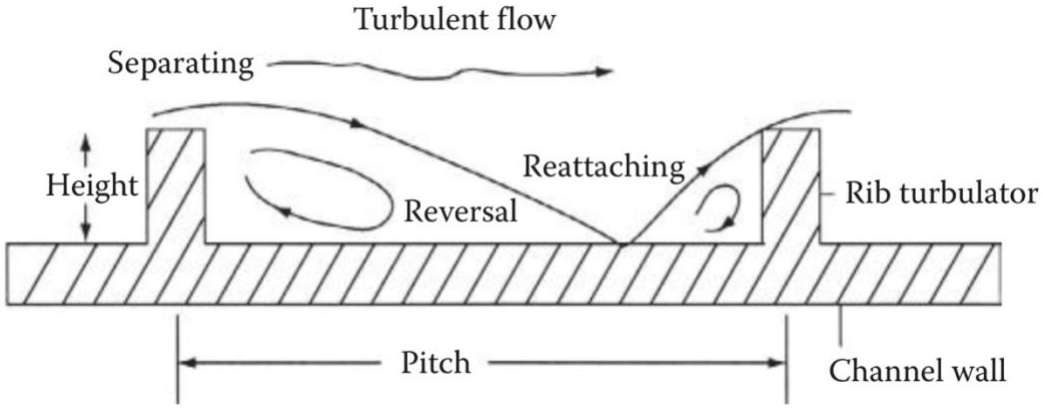

Figure 1.3. Schematic of flow separation and rib orientations in heat-transfer coefficient enhancement [8]

1.3 Effect of Rib-Turbulator in Coolant Flow

An example flow separation and reattachment in rib-turbulated channel is given in Figure 3. Separation occurs upstream and downstream of ribs. In several studies, there was another separation region just above the rib. The flow separates starting from the rib,

reduces the thickness of the boundary layer, and reattaches itself to the heat transfer surface. As a result, near surface fluid can get mixed with the coolant and dissipate effectively increasing the heat transfer coefficient.

CHAPTER 2: LITERATURE REVIEW

2.1 Previous Research

Before nineties, there were many data available in the literature about channel flow with transverse ribs. But in the last three decades, the effect of angled-rib was in consideration when analyzing heat transfer augmentation.

The research work on rib-roughened channel by Taslim et al. showed the effect of ribs on heat transfer coefficient and friction factor. They concluded that roughening the walls with ribs enhanced heat transfer coefficient and increased friction factor. But the net effect is an increment of thermal performance.

Han et al. [9] and Han and Park [10] investigated the effect of Reynolds number, rib geometry and combined effect of channel aspect ratio and rib geometry on local values of heat transfer and pressure drop. Their results indicate angled ribs and lower aspect ratio channels perform better compared to transverse ribs and higher aspect ratio channels.

Peng et al. [11] studied convective heat transfer in a rectangular channel with transverse and angled ribs experimentally and also numerically using SST k-ω turbulence model. They used continuous and interrupted ribs for transverse and different angled ribs and found out that 45° V-shaped continuous ribs had the best thermal performance. In case of V-shaped ribs, continuous ribs had better heat transfer than interrupted ribs. The opposite was true for transverse ribs.

A similar research was also conducted by Taslim et al. [12] with angled, V-shaped and discrete ribs. From the experimental results, it was concluded that 45° ribs

had higher thermal performance than V-shaped and transverse ribs. It was also observed that friction factors of 45° ribs were lower than V-shaped ribs.

Kiml et al [13] investigated heat transfer and pressure drop characteristics of a rectangular channel with 90°, 75°, 60° and 45° ribs and found that highest mean heat transfer was obtained by using 60° ribs. Highest friction coefficient was obtained for 45° parallel rib pattern.

Taslim et al. [14] performed parametric investigation to determine experimentally the effects of turbulator spacing and profile. This research showed that there is an optimum turbulator spacing for a given turbulator blockage ratio (e/D_h) and aspect ratio (AR) and convective heat transfer decreases as AR of ribs decreases. It was also concluded that if aspect ratio of the rib (AR_t) or pitch-to-height ratio (S/e) approaches zero keeping one of the variables (AR_t or S/e) constant then heat transfer co-efficient approaches that of a channel flow without ribs.

Ahn and Lee [15] investigated the thermal performance of detached rib array by using large eddy simulations of turbulent flow. Their purpose was to improve local deterioration of heat transfer behind the rib because of flow separation. However, they discovered that detached rib array provided lower thermal performance than the attached rib array because and also it also increased the pressure drop.

Chompookham et al. [16] studied the heat transfer characteristics of winglet vortex generators (WVGs) and wedge ribs. They used a channel with aspect ratio of 10 and blockage ratio of 0.2 and pitch-to-height ratio of 1.33. They experimented on inline and staggered WVGs with wedge pointing upstream and downstream. The results of this

work showed that combination of staggered wedge rib and WVGs augmented the heat transfer better than the combination of inline wedge rib and WVGs.

There was a similar research performed by Promvonge et al. [17] with triangular (isosceles) ribs and vortex generators. Their blockage ratio was 0.13 and other variables such as aspect ratio of the channel, pitch-to-height ratio were the same as the last research. However, results of this research showed that combination of inline rib and WVGs had better results than the combination of staggered rib and WVGs.

Sripattanapipat and Promvonge [18] analyzed the heat transfer of laminar flow with staggered diamond shaped baffles numerically. They reported that diamond baffle had better enhancement of heat transfer than flat baffles. And 5° diamond baffle had better enhancement factor than diamond baffles of different angles.

Rau et al. [19] investigated heat transfer performance in rib-roughened square duct as a function of rib pitch to height ratio. Blockage ratio of square ribs was 0.10 and 0.20 depending on whether they were inline or staggered. They showed that pitch-to-height ratio of 9 with ribs on the opposite walls provide the best heat transfer enhancement.

Nonino and Comini [20] performed studied convective heat transfer in a square channel using angled ribs. They reported that 45° staggered ribs had the best result. Ahn et al. [21] investigated effect of angled-rib in one, two or four walls of a square channel and found out that one ribbed wall had the maximum heat transfer performance factor than the smooth wall.

Fann et al. [22] studied local heat transfer in a rotating channel with ribs and concluded that the rotation improves the performance. It was also found that the

configuration with 45° ribs with or without rotation of the ribs had better performance than other configurations.

Fu et al. [23] worked on two-pass rotating rectangular channel and showed that for both rotating and non-rotating cases, V-shaped ribs had better heat transfer performance than 45° angled ribs and also 45° angled ribs had the highest friction losses.

Ekkad et al. [24] investigated straight channels with ribs and tapered channels with ribs and concluded that both kind of channels provide similar enhancement. Though local Nusselt number was higher in tapered channels with ribs, Reynolds number increased as well and nullified the taper effect.

Wang and Sundén [25] investigated local heat transfer with square, equilateral-triangular, and trapizoidal ribs with increasing and decreasing height. It was reported that trapizoidal ribs with decreasing height in the direction of aif flow had the highest heat transfer performance and pressure drop.

2.2 Key findings from Previous Research

The important conclusions drawn from the preceding researches relevant to this paper are summarized below:

- Heat transfer coefficient and pressure drop are important factors when evaluating the performance of rib-roughened surface.
- CFD can be a very effective and comparatively inexpensive tool for solving a problem and predicting outcome.
- Heat transfer can be enhanced by increasing the height of ribs (as a result blockage ratio also increases) but it will also increase the pressure drop.

- The distance between two adjacent ribs effects the heat transfer in channel flow.
- Heat transfer enhancement factors varies with Reynolds number depending on the shape of ribs and channel.
- For a given blockage ratio, there is an optimum pitch-to-height ratio for maximum heat transfer.
- Change of angle of rib greatly effects the heat transfer compared to transverse ribs.
- The shape of ribs has significant impact on pressure drop and heat transfer.

2.3 Research Contribution and Objective

Very few data are available in the previous researches for the effect of different shapes of rib on heat transfer and pressure drop. The primary focus of this research is on the different shapes of rib and how it is affecting the nature of flow to have an impact on heat transfer characteristics. Some of the work are derivative of the previous research and while designing the CAD models, the experimental results obtained in the literature was taken into consideration. However, in this paper some of the shapes of rib (e.g. pentagon shape) and arrangement are unique compared to preexisting research.

CHAPTER 3: METHOD AND APPROACH

In this chapter, techniques used to generate CAD models, variables of mesh and physics models used to find solutions were discussed. Experimental results for validation case were presented.

3.1 CAD Model Generation

The CAD models for simulations were generated in STAR-CCM+ CAD. While generating models of different rib shapes, the aspect ratio of the channel and ribs, pitch-to-height ratio, length of the channel were kept the same in order to compare the results accurately.

First, the base for the channel was created on a plane.

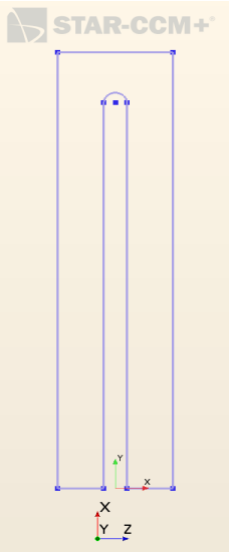

Figure 3.1. The base of model

The sketch of base was extruded to make three-dimensional representation of two-pass the channel.

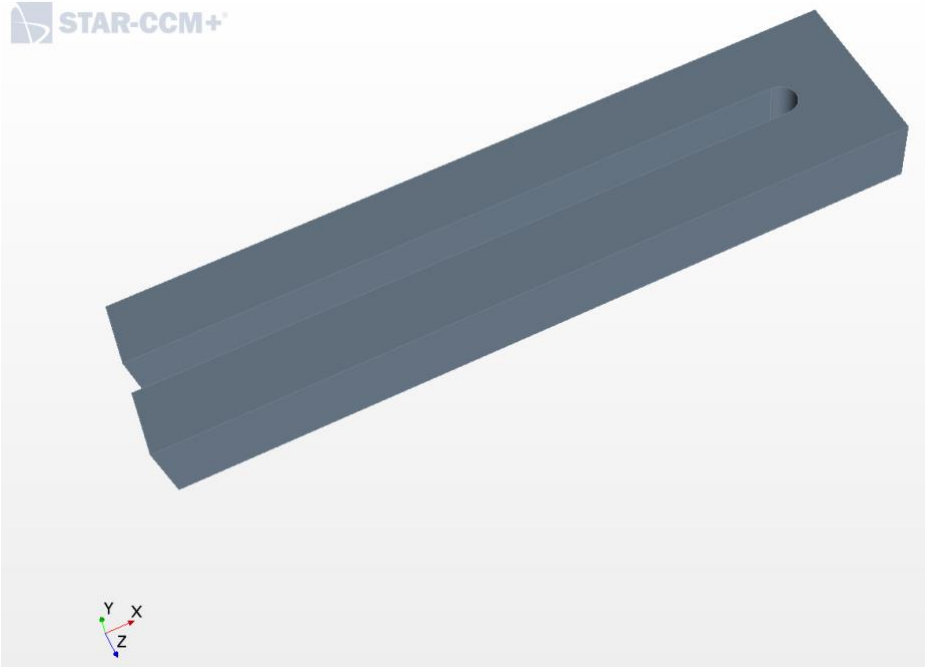

Figure 3.2. Three-dimensional representation by extruding

One of the side walls of channel was transformed to create a plane. The layout for each rib was drawn on transformed plane starting from the inlet and distance between each rib outline was kept the same.

Figure 3.3. Transparent view of model with outline of ribs

Next, for all the ribs layout, extrude cut was made from transformed plane to generate ribbed-roughened wall on the channel.

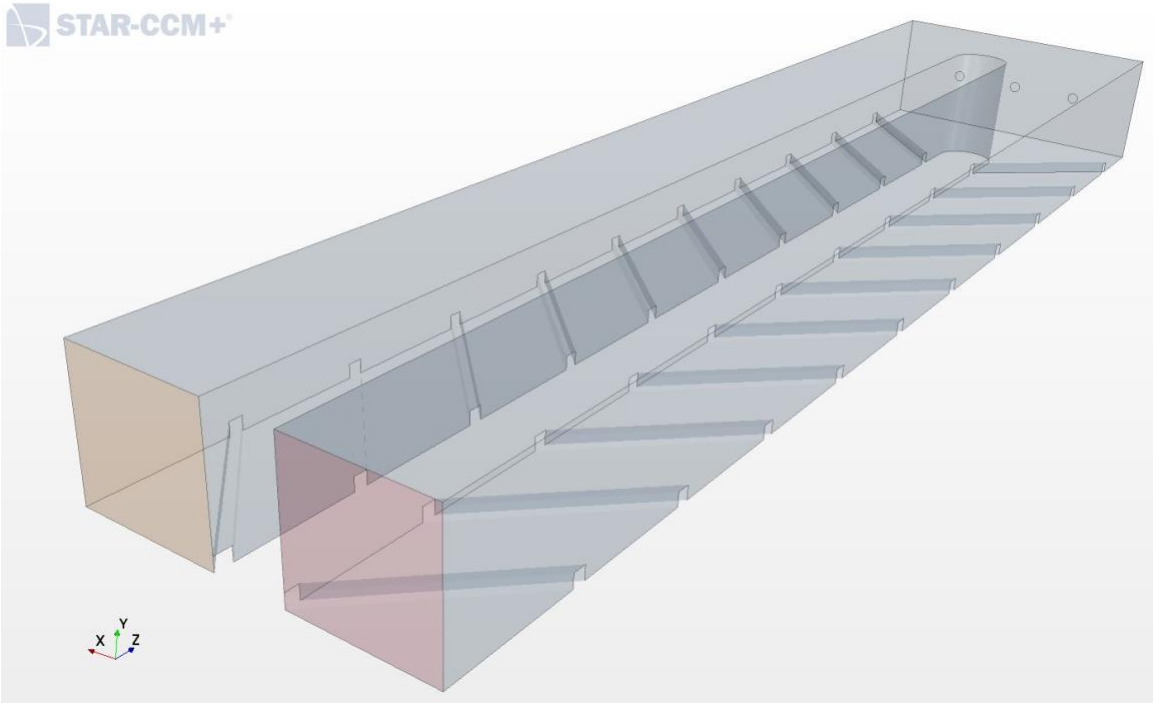

Figure 3.4. Transparent view of 3D CAD model with square ribs

The procedure described above is an example (in this case, the CAD model for validation) of creating a CAD model within StarCCM+ CAD system.

3.2 Discretization

To create discrete representation of the geometry of the problems, polyhedral mesh was used. The base size for all models was the same for ease of comparison. In case of some complicated geometries, custom mesh was required to capture the actual geometry.

Mesh Models:

a) Surface Remesher

b) Surface Wrapper

c) Advancing Layer Mesher

d) Extruder

It was important to generate best possible mesh, so it can discretize the actual geometry and also it is not computationally expensive when running the simulations. Choosing the right variables in this case was done by a lot of trials. The primary variables selected for all geometries are given below:

Base size $= 6*10^{-4}$ m

Number of prism layers $= 15$

Prism layer stretching $= 1.2$

3.3 Fluid Modeling

Physics Models:

a) Three Dimensional
b) Ideal Gas
c) Turbulent
d) Steady
e) Gradients
f) Coupled Flow
g) SST (Menter) K-Omega
h) Reynolds-Averaged Navier-Stokes

The assumptions were made in the physics model based on experiments in order to replicate the experimental conditions. Velocity of air at the inlet depended on Reynolds number (Re) and hydraulic diameter (D_h) of the channel. The value of dynamic viscosity (μ) and density (ρ) of air was used at standard conditions. Because Reynolds number was higher than 4,000, the flow was assumed to be turbulent. Air behaves effectively as an ideal gas at standard conditions and for that reason in physics model

ideal gas was selected. The rib-roughened wall was subjected to constant heat flux of 3000 W/m^2.

Hydraulic diameter of the channel was calculated using the following formula:

$$D_h = \frac{4A}{P} \qquad (1)$$

A = Cross-sectional area of inlet

P = Perimeter of inlet

Velocity at the inlet of the channel was calculated at Re = 25,000 using the formula given below:

$$Re = \frac{\rho v D_h}{\mu} \qquad (2)$$

The variables in the default settings of the software package was changed to reproduce experimental setup. The primary variable changed in the settings are given below:

Heat Flux = 3000 W/m^2

Hydraulic Diameter, D_h = 20 mm

Inlet Velocity, v = 19.6 m/s

3.4 Governing Equations

Governing equations for our simulations was Navier-Stokes equations which gave numerical solution to the problems. Built-in equations in STAR-CCM+ were used to predict the characteristics of the channel flow. The simulations presented in this paper used Reynolds-averaged Navier-Stokes equations (RANS equations) which give approximate time-averaged solutions.

Vector form of Navier-Stokes equations:

$$\frac{\partial \rho}{\partial t} + \nabla(\rho \boldsymbol{u}) = 0 \quad (3)$$

$$\frac{\partial u}{\partial t} + (\boldsymbol{u}\nabla)\boldsymbol{u} = -\frac{1}{\rho}\nabla\rho + F + \frac{\mu}{\rho}\nabla^2\boldsymbol{u} \quad (4)$$

$$\rho\left(\frac{\partial \varepsilon}{\partial t} + \boldsymbol{u}\nabla\varepsilon\right) - \nabla(K_H \nabla T) + \rho\nabla\boldsymbol{u} = 0 \quad (5)$$

where, $\nabla(\,) = \boldsymbol{i}\frac{\partial}{\partial x} + \boldsymbol{j}\frac{\partial}{\partial y} + \boldsymbol{k}\frac{\partial}{\partial z}$ (6)

3.5 Validation Case

Before conducting simulations with different shapes of ribs and angle of attack (α), it was necessary to justify the reason for selecting such geometry, physics conditions. So, experimental results from previous researchers were used to validate simulation results presented in this paper.

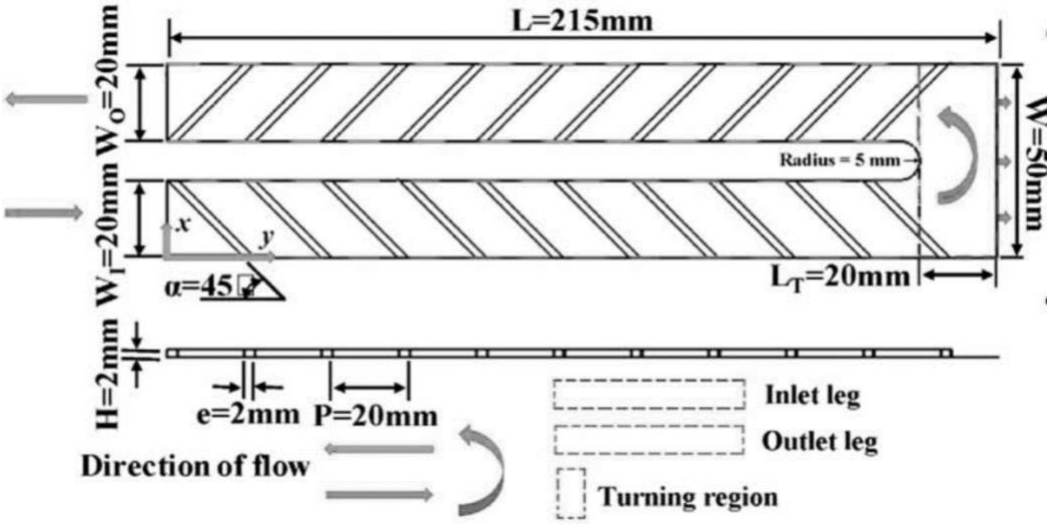

Figure 3.5. Geometry specifications of validation case [26]

A case for validation was chosen based on one of the experimental results from Chang and Cai's [26] research on heat transfer and pressure drop in two-pass rib-roughened channel with bleed from sharp bend. The result that was used to validate the

simulation was square channel with square ribs at $\alpha = 45°$ with no bleed from the sharp bend and *Re* = 25,000.

Taslim et al. [12] found in experiments about channel roughened with different angled (α) ribs that highest thermal performance occurred at $\alpha = 45°$. This result will be used to validate for optimum angle for best heat transfer performance by using results from simulations.

CHAPTER 4: RESULT AND DISCUSSION

In this chapter, all the results from simulations will be presented including the validation case. For validation case, simulations were done with two-pass square channel. Then the geometry was simplified to a one-pass square channel. As a result, it reduced the time to run the simulations because the volume of the channel was reduced. It simplified the process of CAD model generation and mesh generation. And also, the effect of sharp bend in two-pass channel was eliminated. So, the simplification of the geometry reduced the computation time and allowed the focus of this research to be solely on the shape of rib.

4.1 Validation Case Results

The CAD model and simulation results for the validation case are presented below. The contour plots of temperature, pressure and Nusselt number will indicate reliability of the simulations.

The percent difference between the experimental result [26] and numerical simulation result of rib-roughened surface average of Nusselt number is about 20% and produce a good validation case for square channel with rib simulations. The reason for this difference in experimental and simulation results can be attributed to the assumption made in the physics conditions and mesh quality. The unsteady nature of the flow was not reflected in the RANS simulations. This limitation can be overcome by Large Eddy Simulation (LES) simulations. But the this would increase the computation time drastically and simulations would be too expensive to run.

The same physics condition and mesh variables used in the validation case was applied to one-pass rib-roughened square channels with different rib shapes.

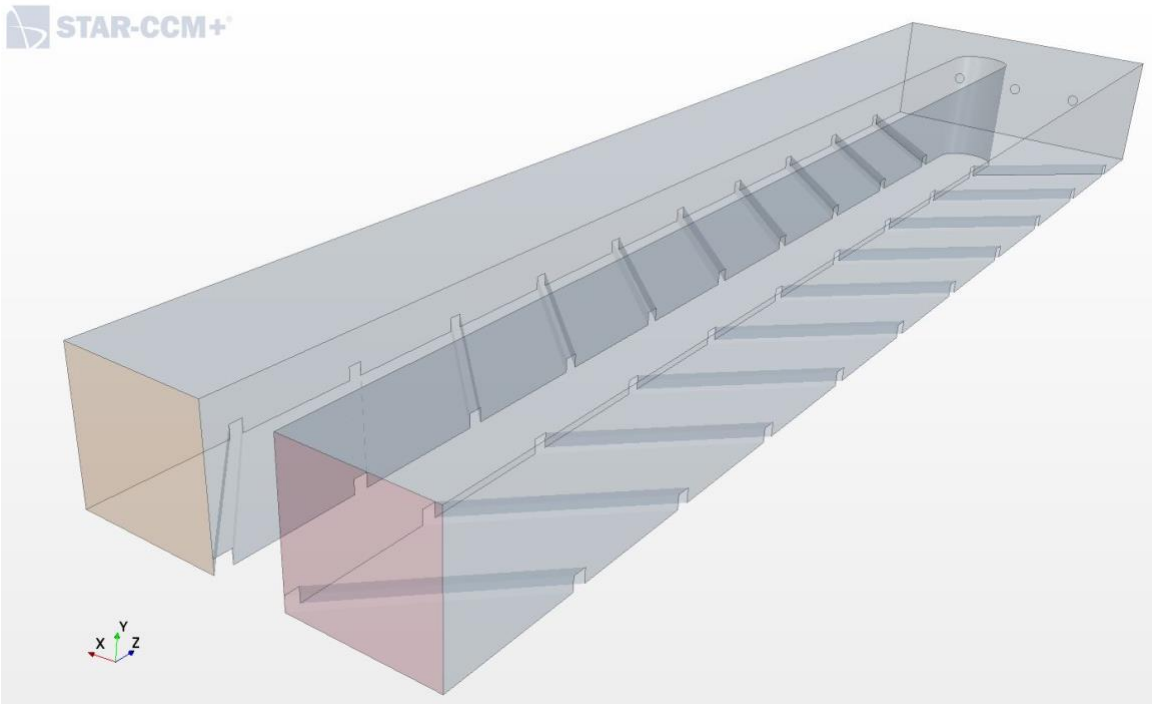

Figure 4.1. Two-pass square channel with 45° square ribs CAD model for validation

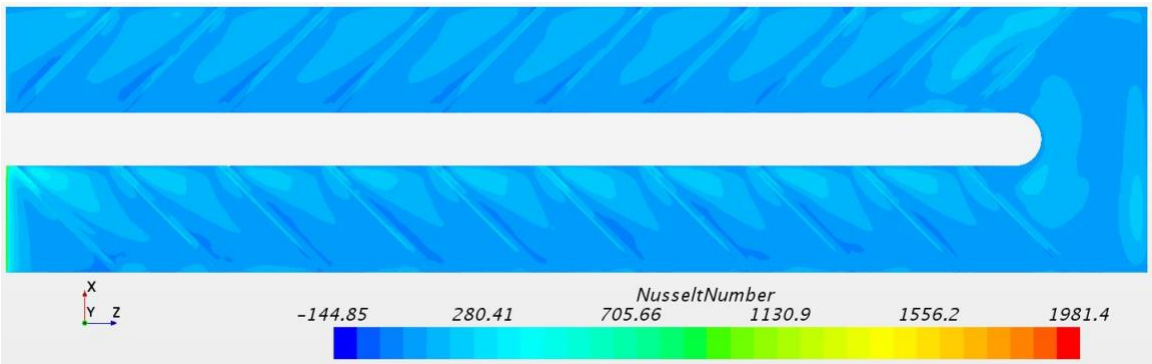

Figure 4.2. Nusselt number contour plot for two-pass rib-roughened square channel

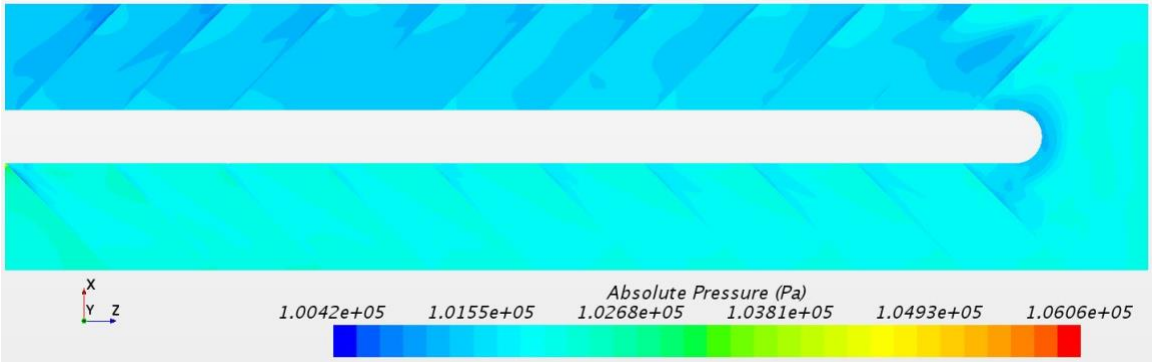

Figure 4.3. Absolute pressure contour plot for two-pass rib-roughened square channel

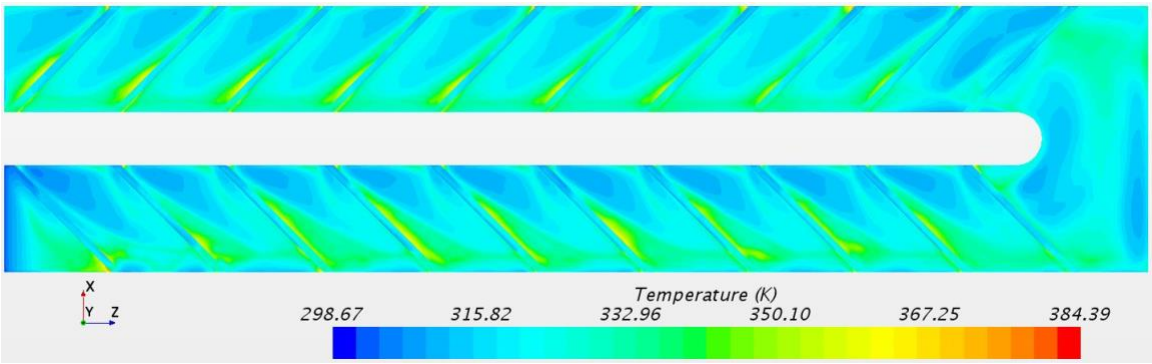

Figure 4.4. Temperature contour plot for two-pass rib-roughened square channel

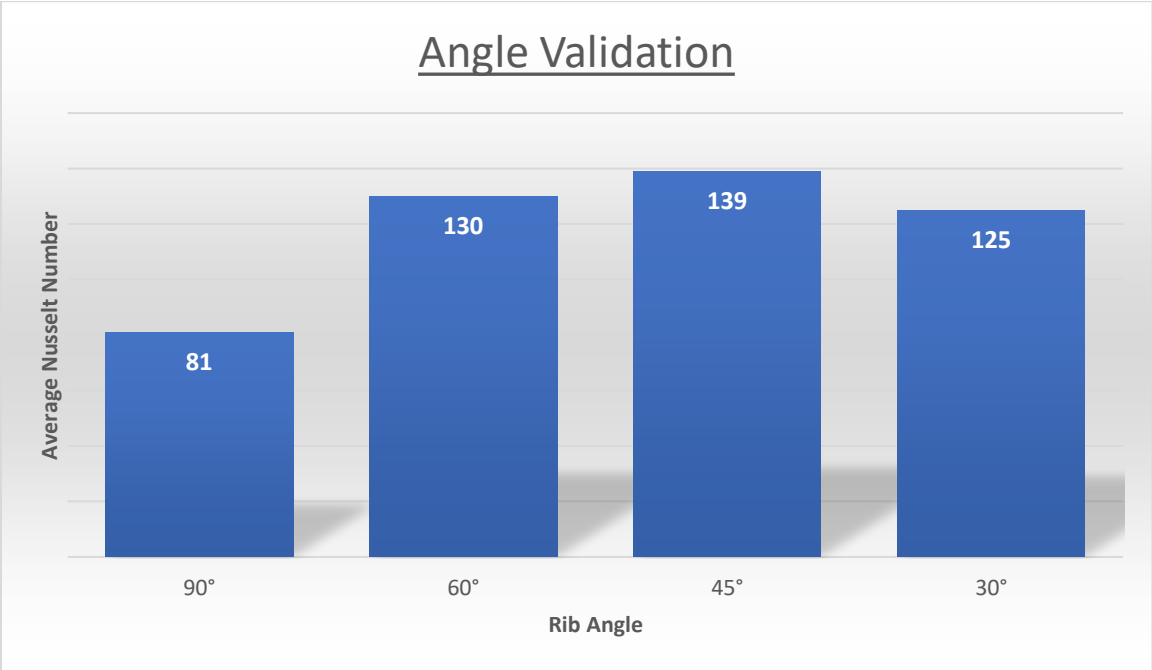

Figure 4.5. Average Nusselt number in square rib-roughened channel with different angles

The optimum angle of rib-roughened square channel was found to be 45° from simulations and this result is backed up by the experimental result from the previous research [12]. So, it also serves as a validation case for optimum angle of rib for maximum heat transfer.

4.2 Square Rib Results

4.2.1 Transverse Square Rib Results

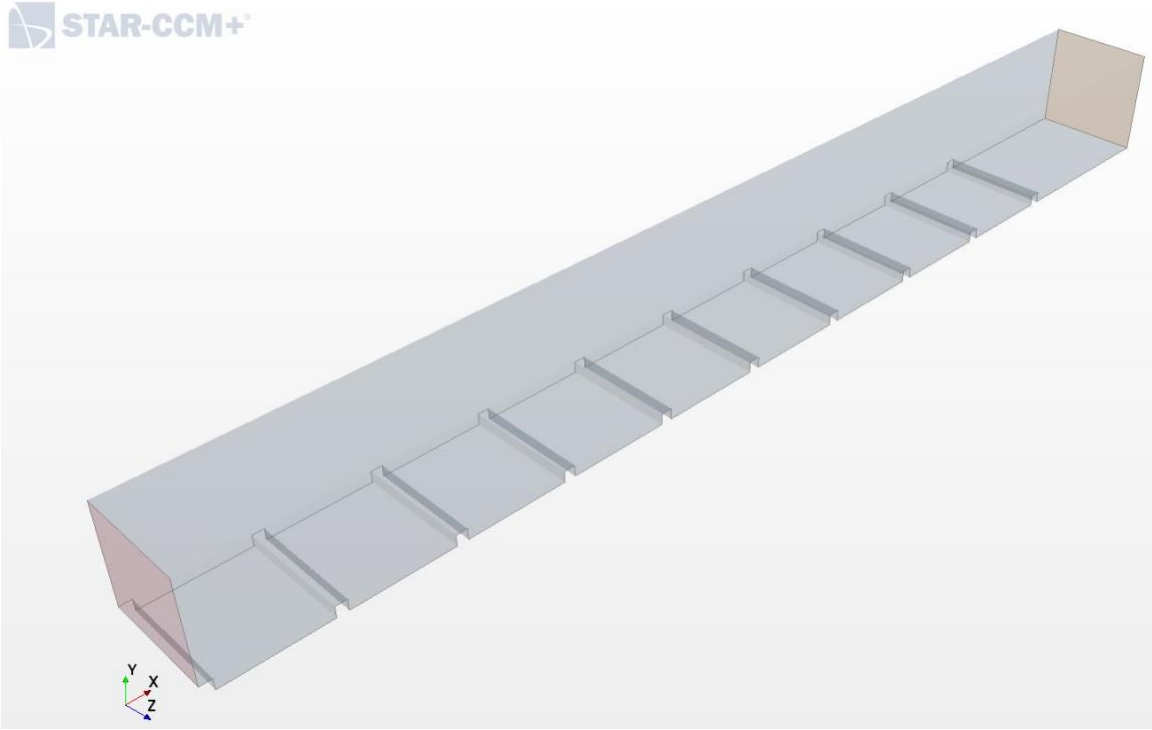

Figure 4.6. CAD model of transverse square ribs

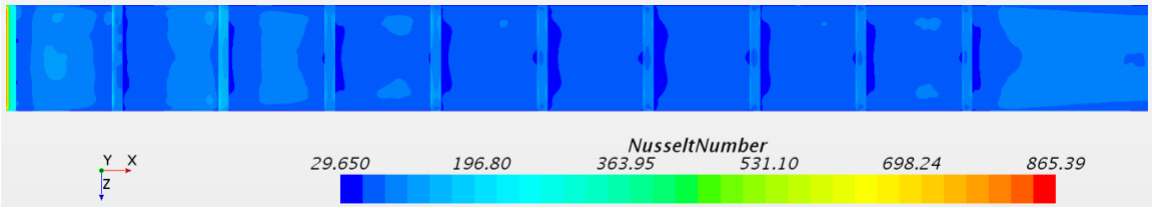

Figure 4.7. Nusselt number contour plot for transverse square rib

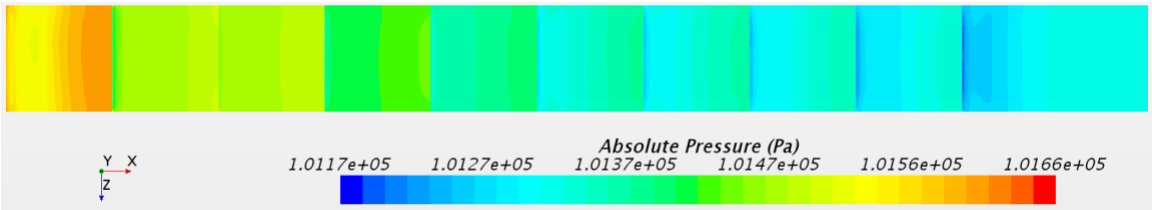

Figure 4.8. Absolute pressure contour plot for transverse square rib

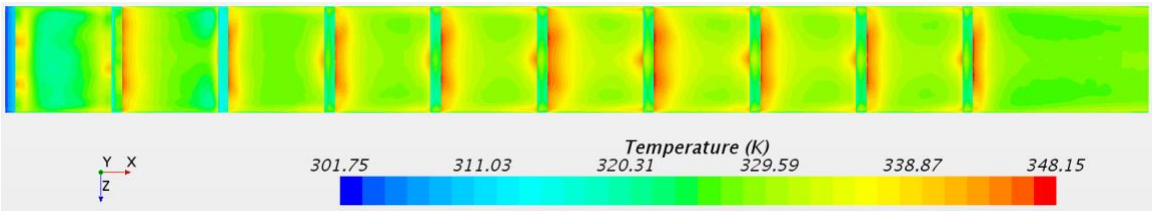

Figure 4.9. Temperature contour plot for transverse square rib

4.2.2 45° Square Rib Results

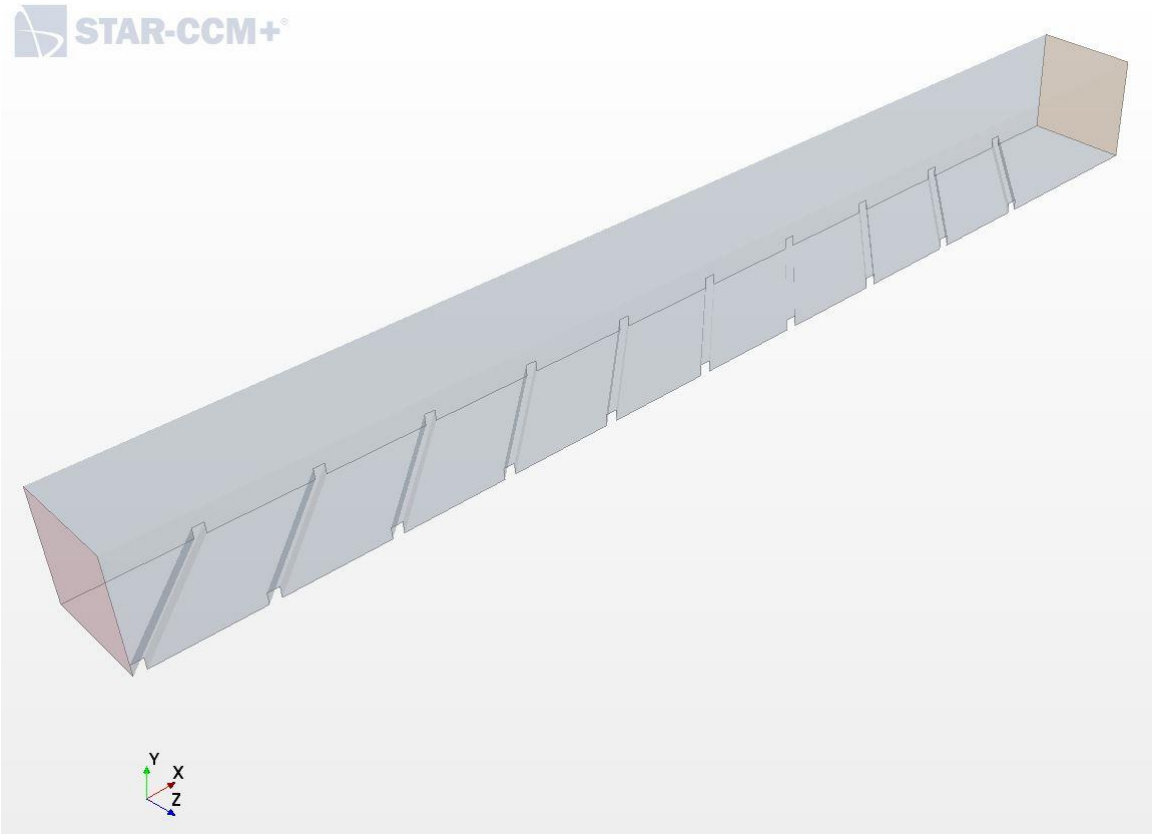

Figure 4.10. CAD model of 45° square ribs

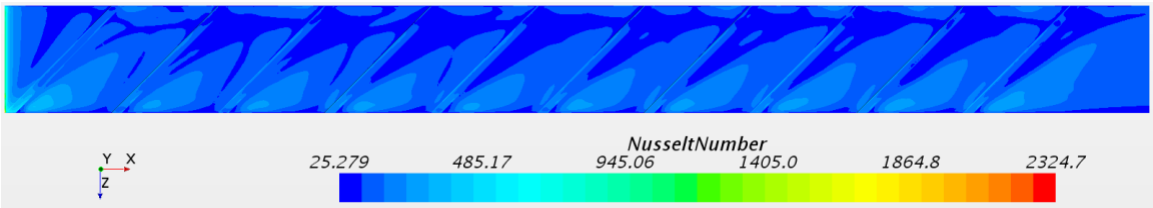

Figure 4.11. Nusselt number contour plot for 45° square rib

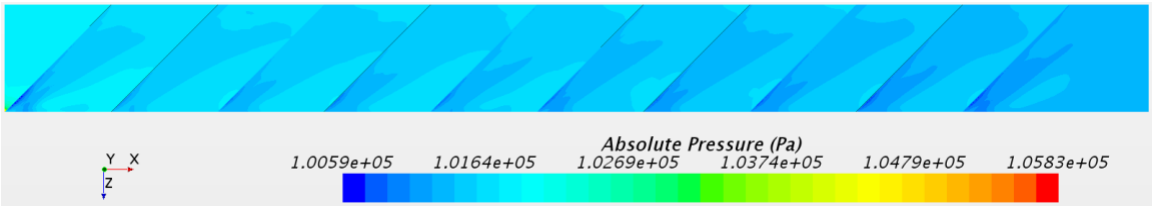

Figure 4.12. Absolute pressure contour plot for 45° square rib

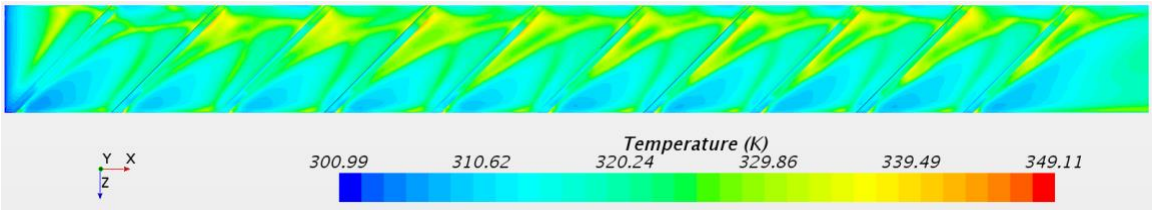

Figure 4.13. Temperature contour plot for 45° square ribs

4.3 Isosceles Triangular Rib Results

4.3.1 Transverse Isosceles Triangular Rib Results

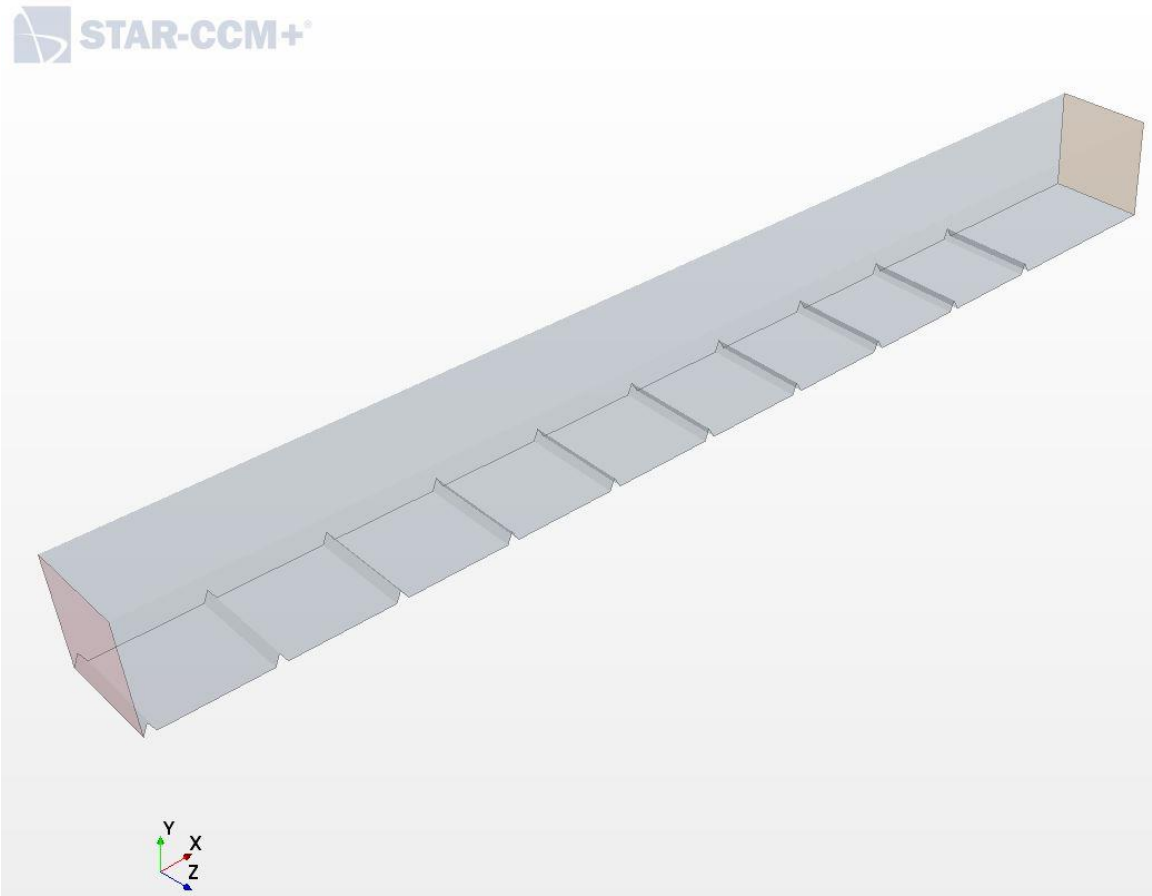

Figure 4.14. CAD model of transverse isosceles triangular ribs

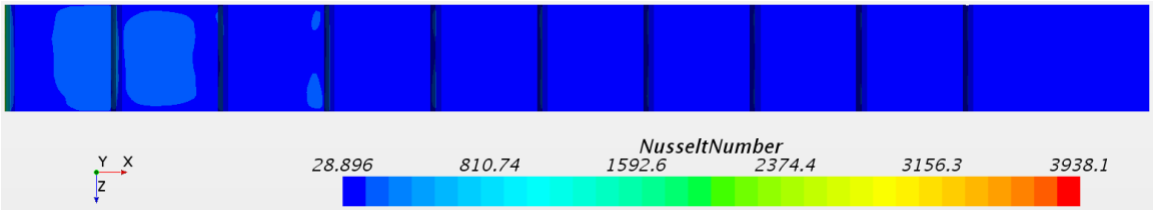

Figure 4.15. Nusselt number contour plot for transverse isosceles triangular rib

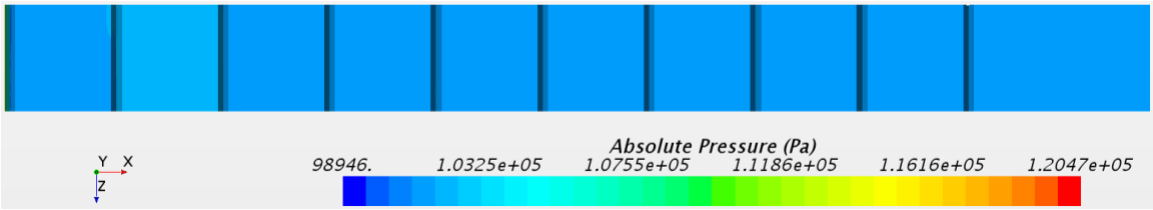

Figure 4.16. Absolute pressure contour plot for transverse isosceles triangular rib

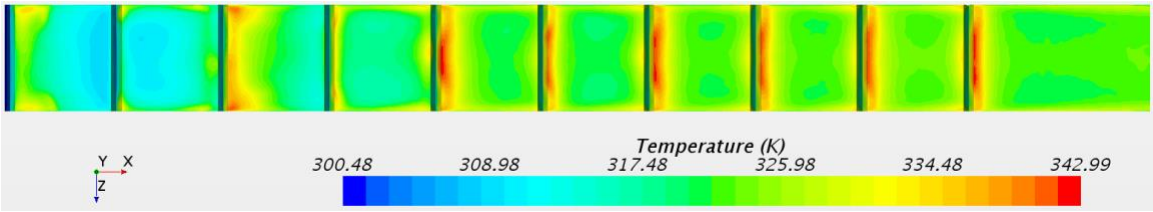

Figure 4.17. Temperature contour plot for transverse isosceles triangular rib

4.3.2 45° Isosceles Triangular Rib Results

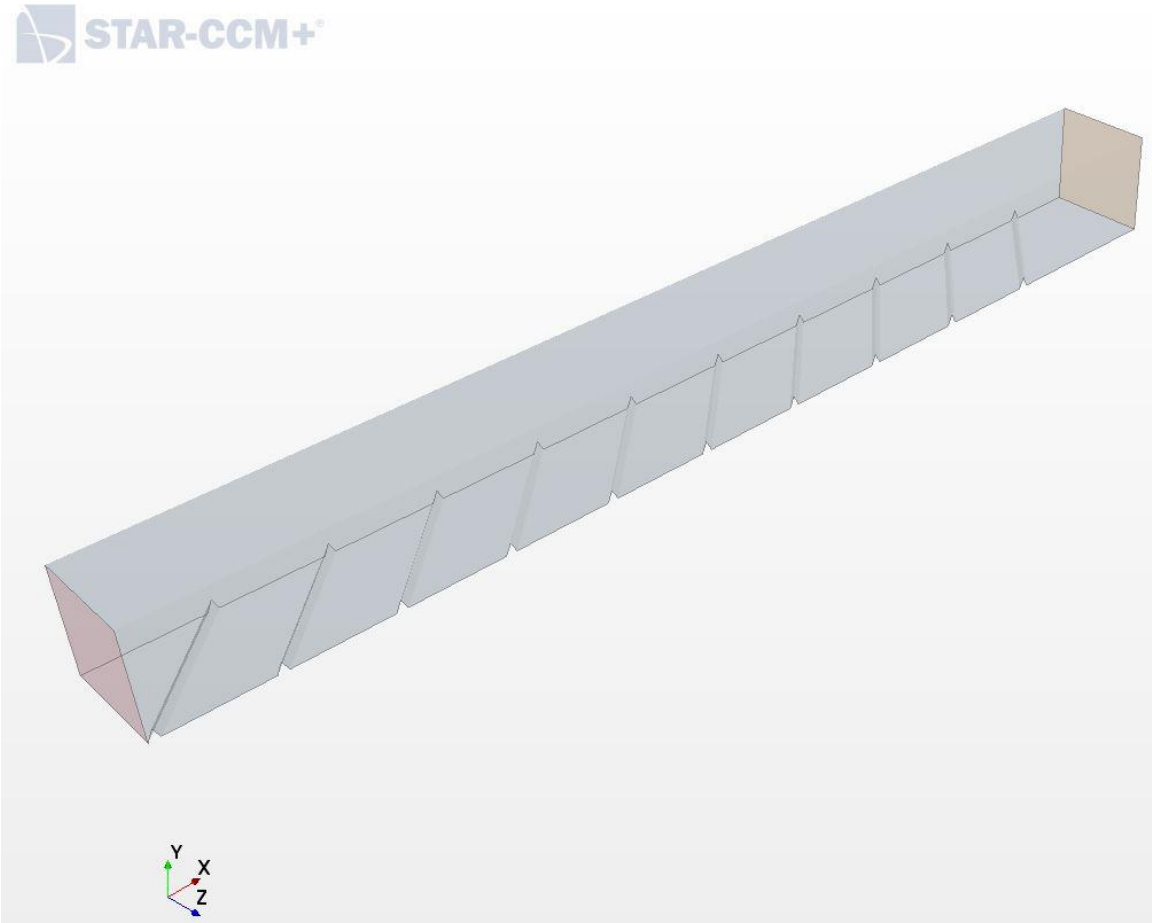

Figure 4.18. CAD model of 45° isosceles triangular ribs

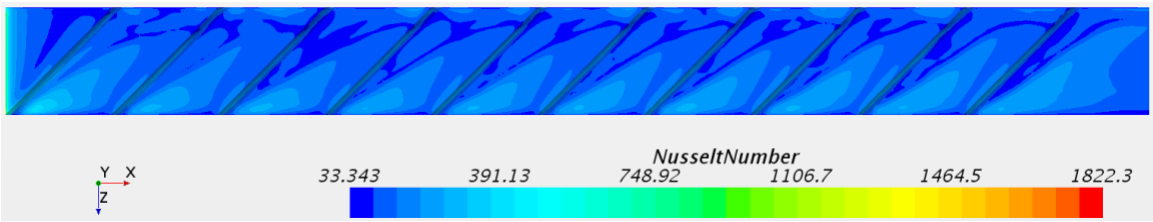

Figure 4.19. Nusselt number contour plot for 45° isosceles triangular rib

Figure 4.20. Absolute pressure contour plot for 45° isosceles triangular rib

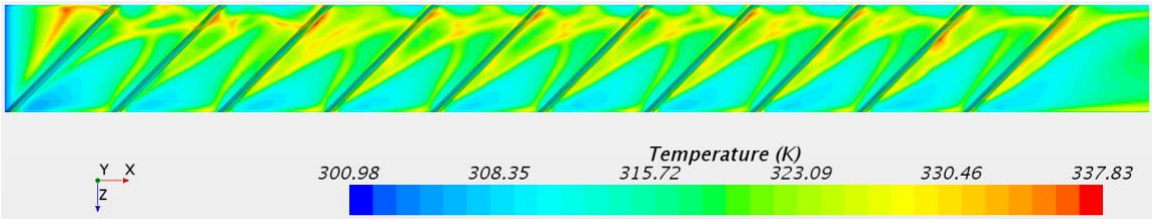

Figure 4.21. Temperature contour plot for 45° isosceles triangular rib

4.4 Pentagon Rib Results

4.4.1 Transverse Pentagon Rib Results

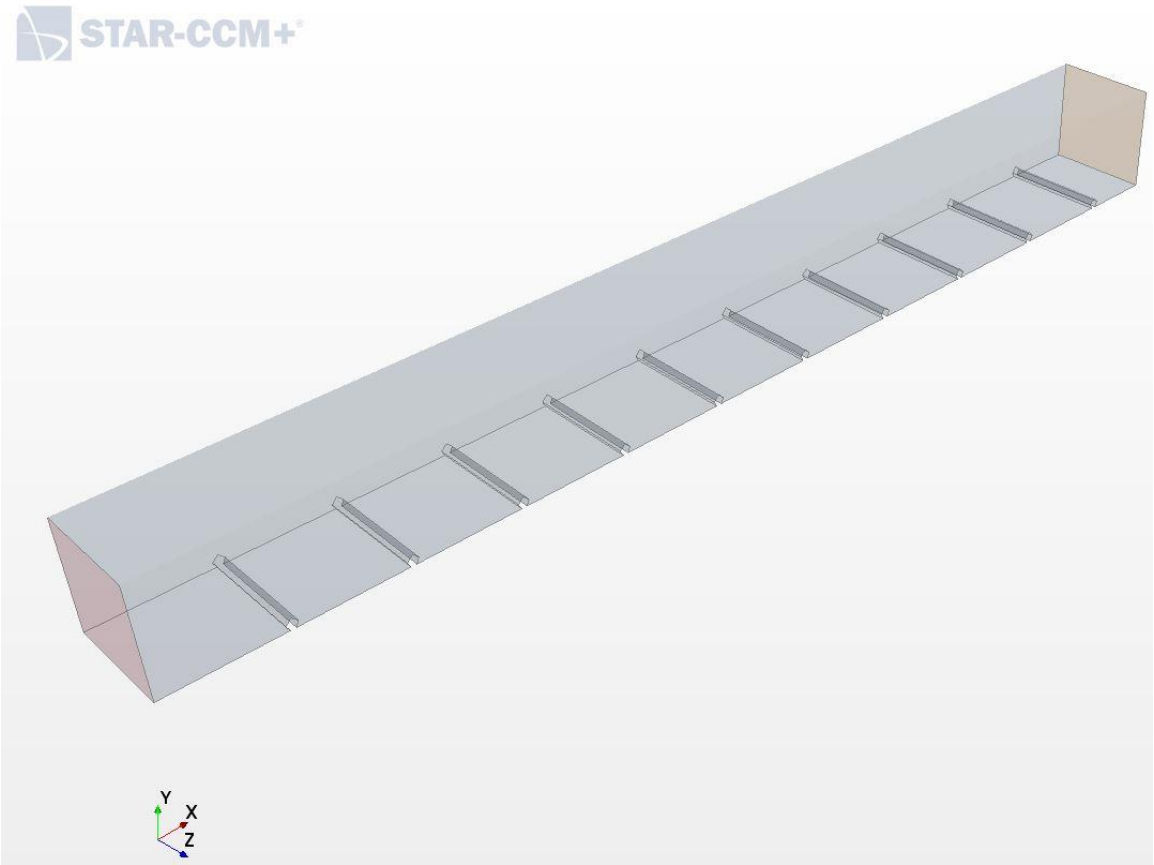

Figure 4.22. CAD model of transverse pentagon ribs

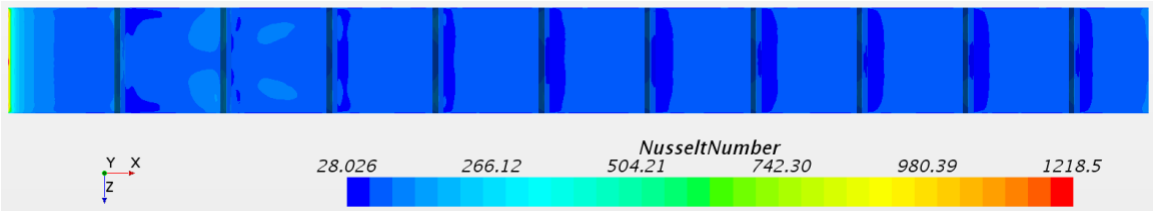

Figure 4.23. Nusselt number contour plot for transverse pentagon rib

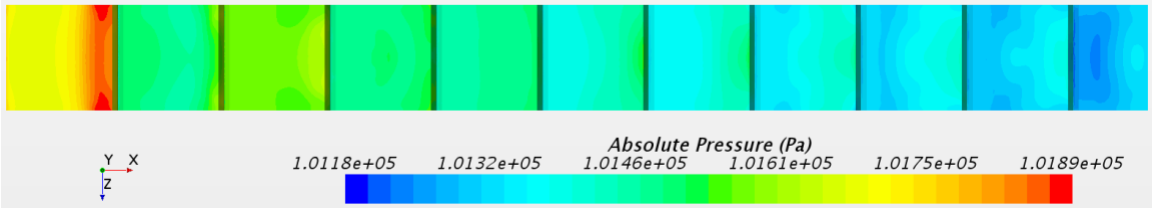

Figure 4.24. Absolute Pressure contour plot for transverse pentagon rib

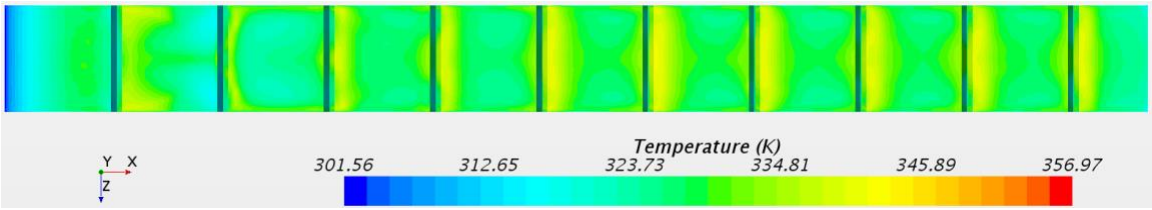

Figure 4.25. Temperature contour plot for transverse pentagon rib

4.4.2 45° Pentagon Rib Results

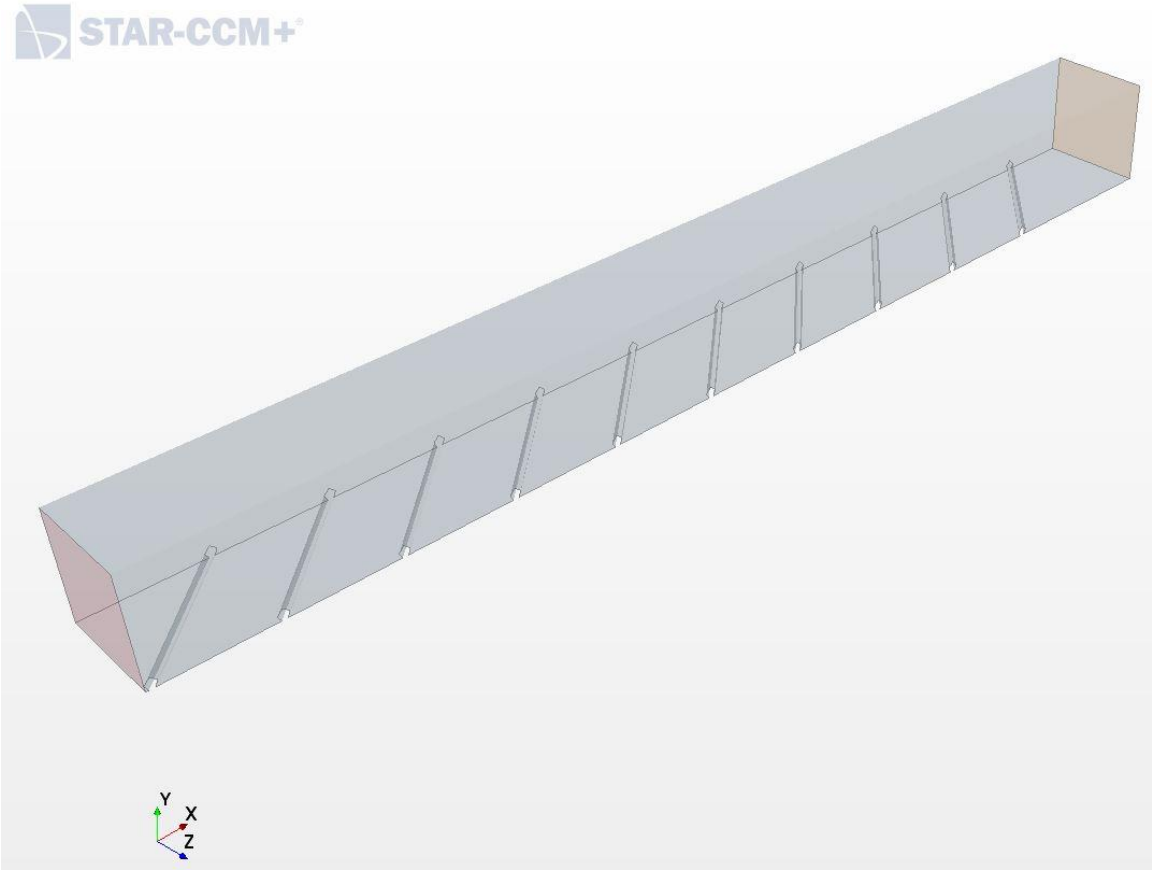

Figure 4.26. CAD model of 45° pentagon ribs

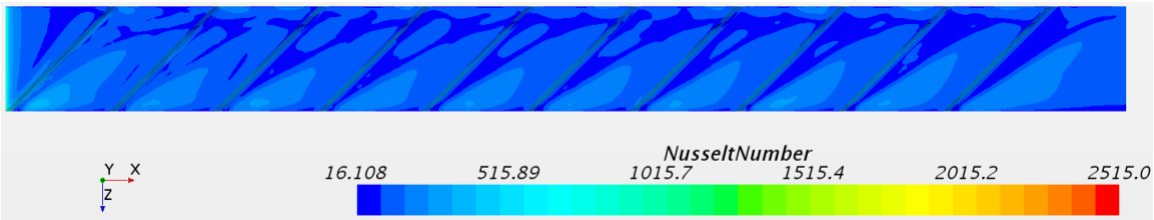

Figure 4.27. Nusselt number contour plot for 45° pentagon rib

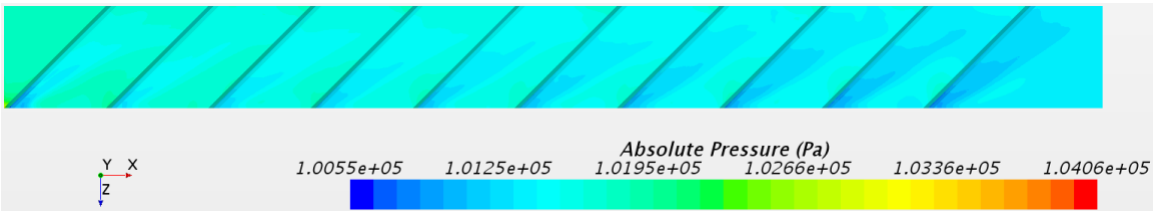

Figure 4.28. Absolute Pressure contour plot for 45° pentagon rib

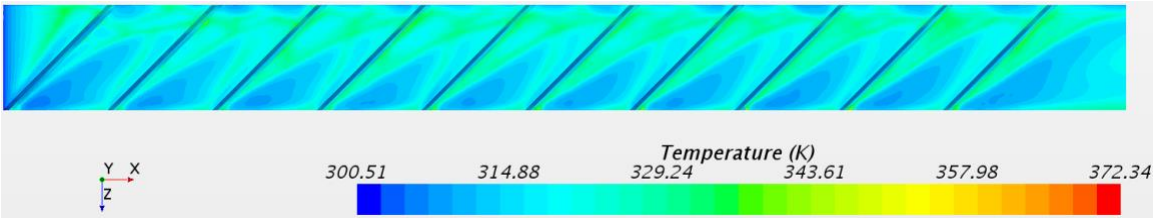

Figure 4.29. Temperature contour plot for 45° pentagon rib

4.5 Right Triangular Rib Pointing Downstream Results

4.5.1 Transverse Right Triangular Rib Pointing Downstream Results

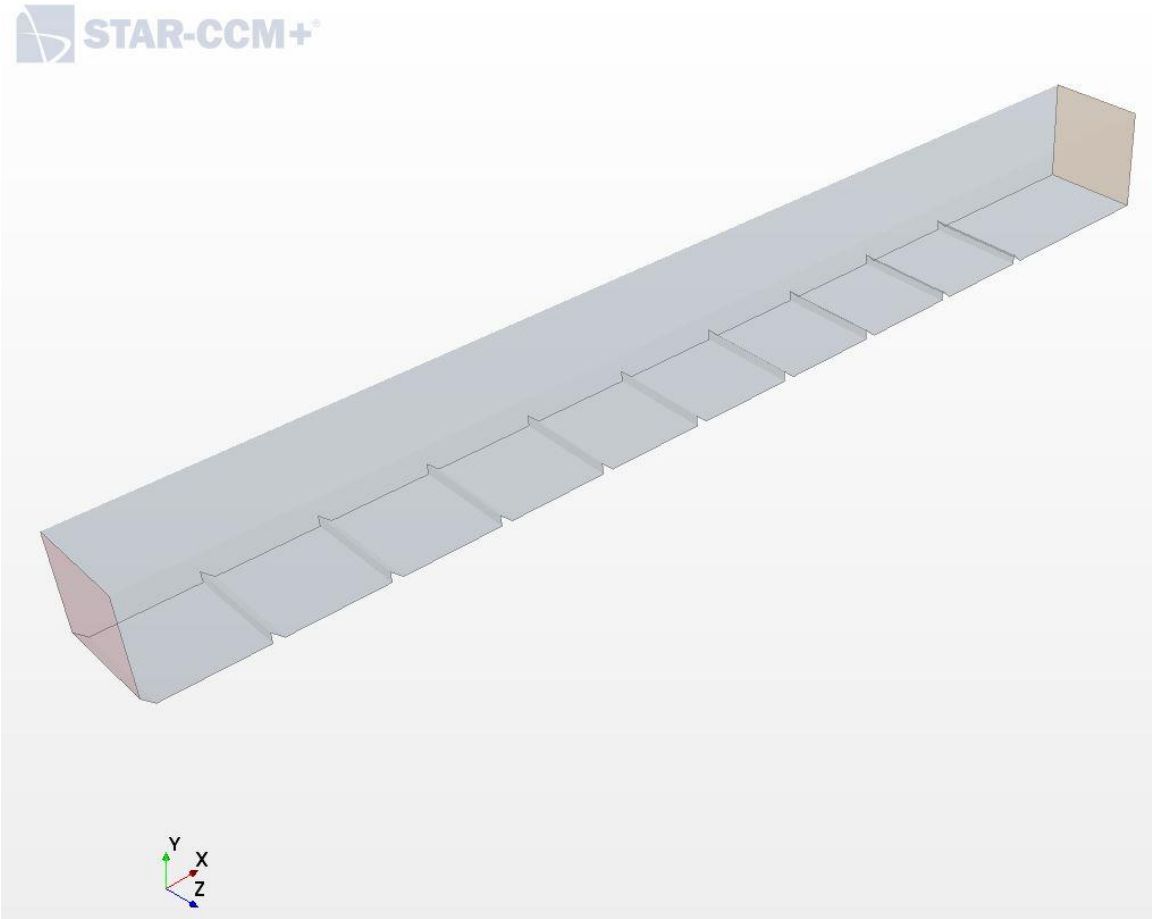

Figure 4.30. CAD model of transverse right triangular rib pointing downstream

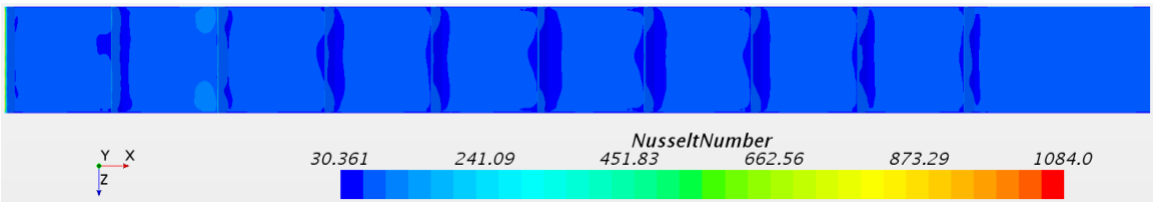

Figure 4.31. Nusselt number contour plot for transverse right triangular rib pointing downstream

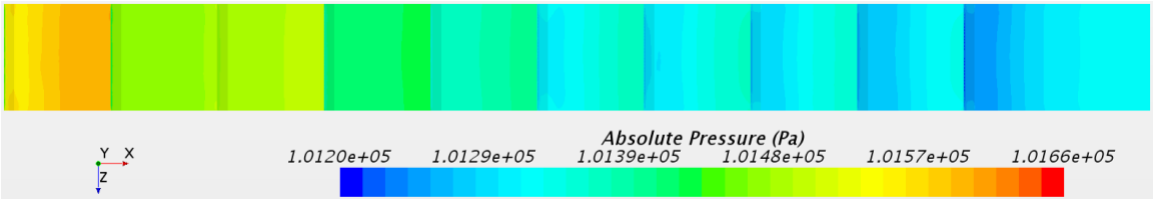

Figure 4.32. Absolute Pressure contour plot for transverse right triangular rib pointing downstream

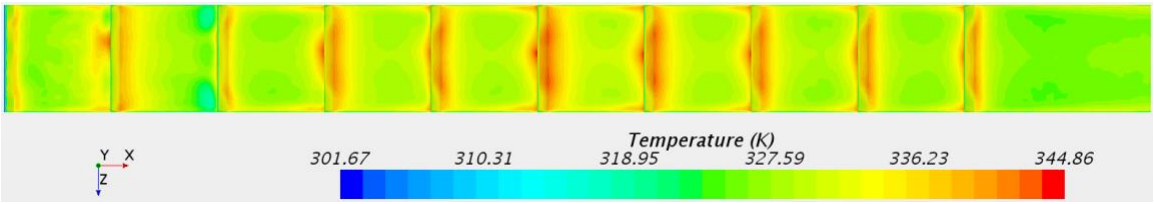

Figure 4.33. Temperature contour plot for transverse right triangular rib pointing downstream

4.5.2 45° Right Triangular Rib Pointing Downstream Results

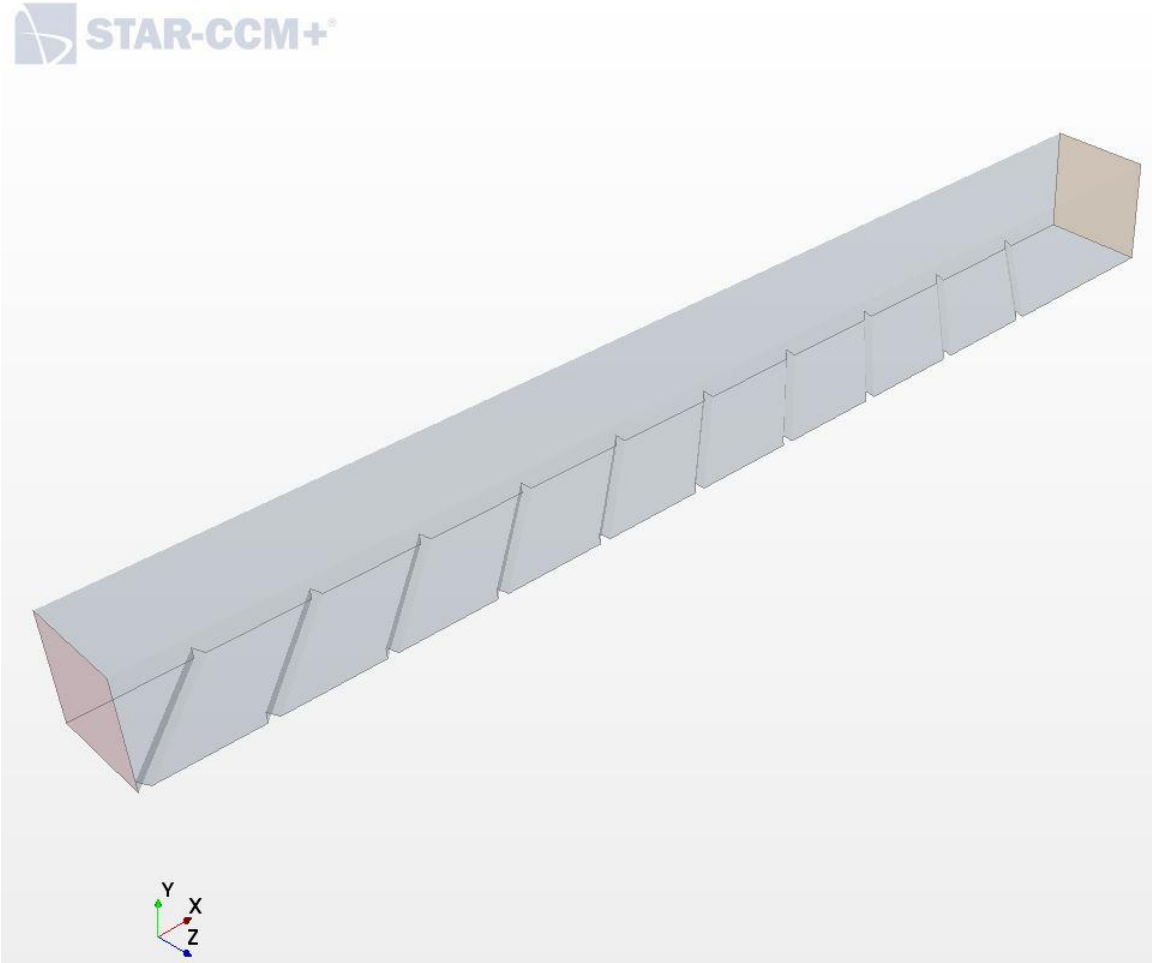

Figure 4.34. CAD model of 45° right triangular rib pointing downstream

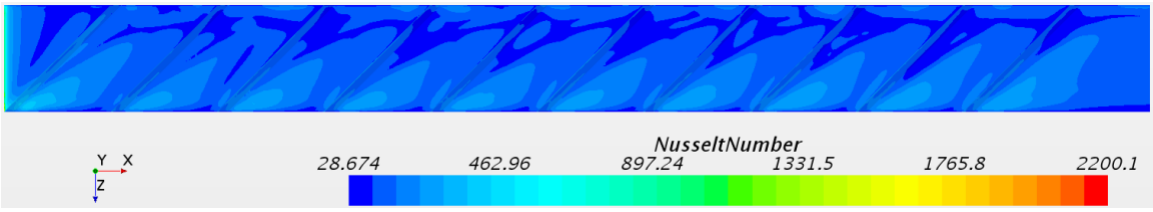

Figure 4.35. Nusselt number contour plot for 45° right triangular rib pointing downstream

Figure 4.36. Absolute Pressure contour plot for 45° right triangular rib pointing downstream

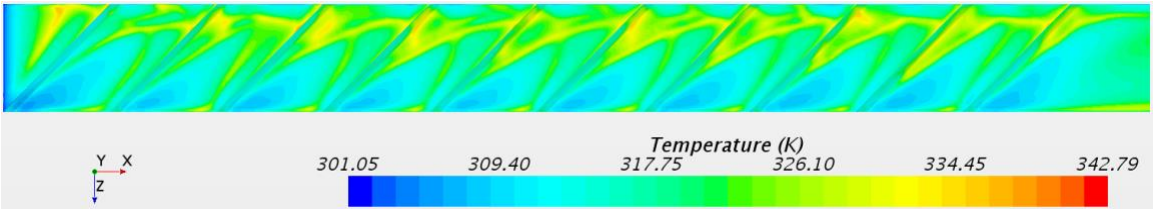

Figure 4.37. Temperature contour plot for 45° right triangular rib pointing downstream

4.6 Right Triangular Rib Pointing Upstream Results

4.6.1 Transverse Right Triangular Rib Pointing Upstream Results

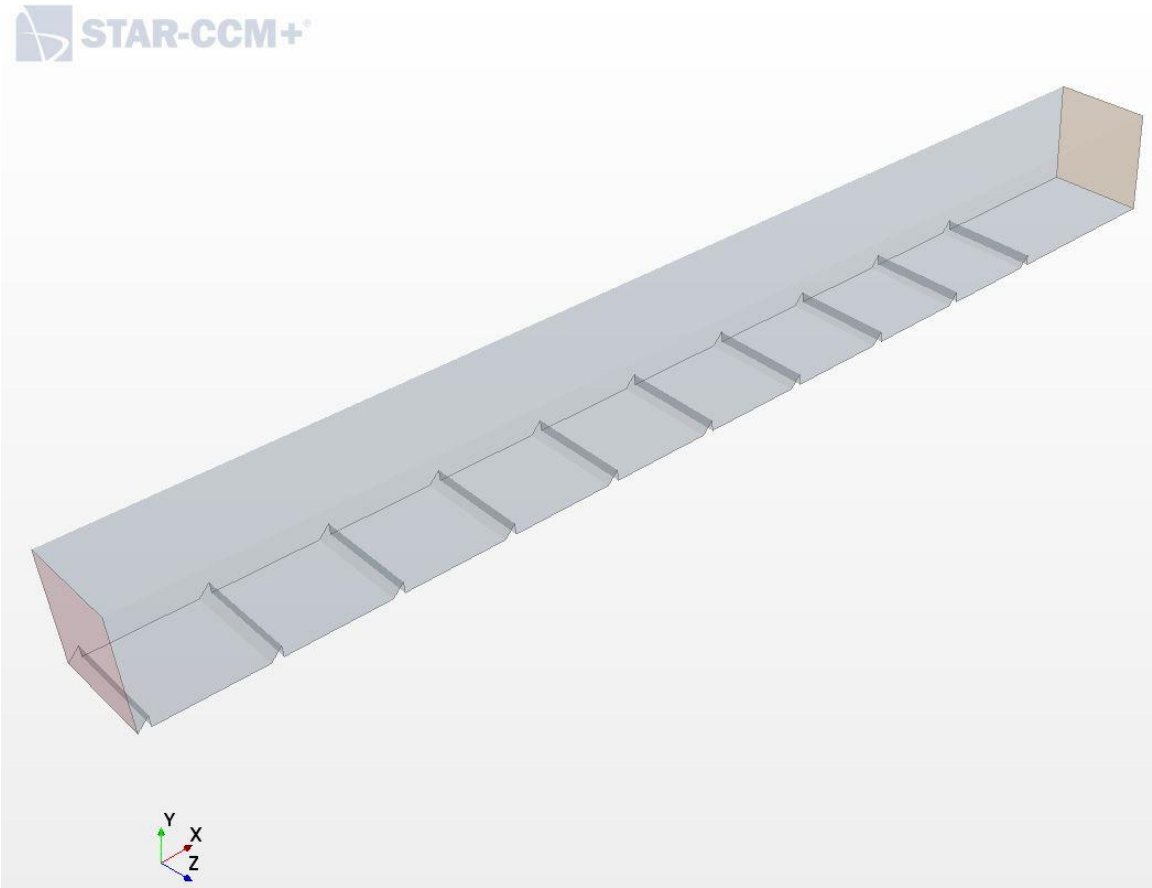

Figure 4.38. CAD model of transverse right triangular rib pointing upstream

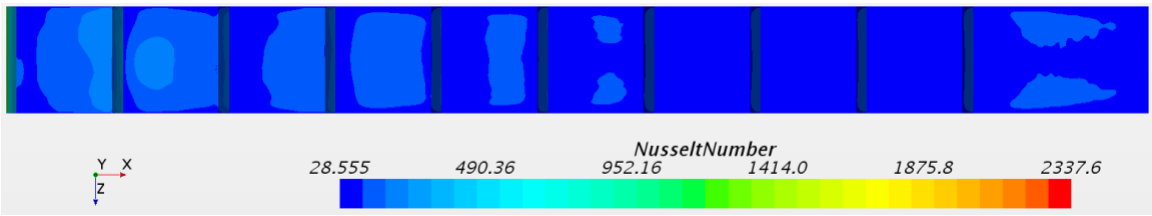

Figure 4.39. Nusselt number contour plot for transverse right triangular rib pointing upstream

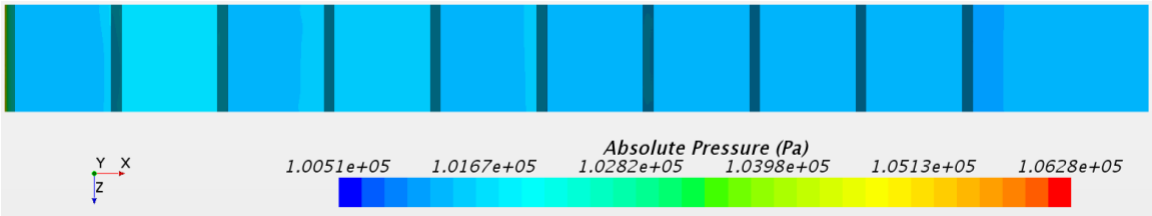

Figure 4.40. Absolute Pressure contour plot for transverse right triangular rib pointing upstream

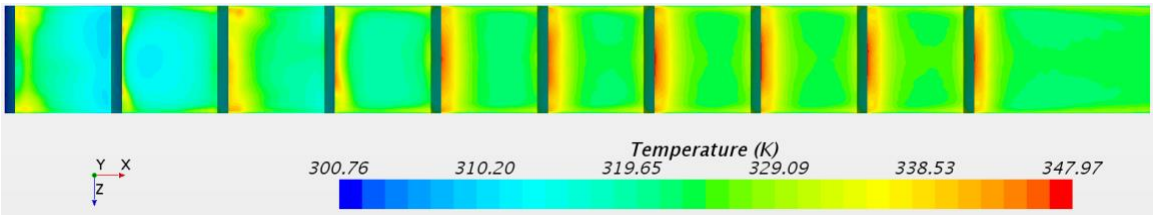

Figure 4.41. Temperature contour plot for transverse right triangular rib pointing upstream

4.6.2 45° Right Triangular Rib Pointing Upstream Results

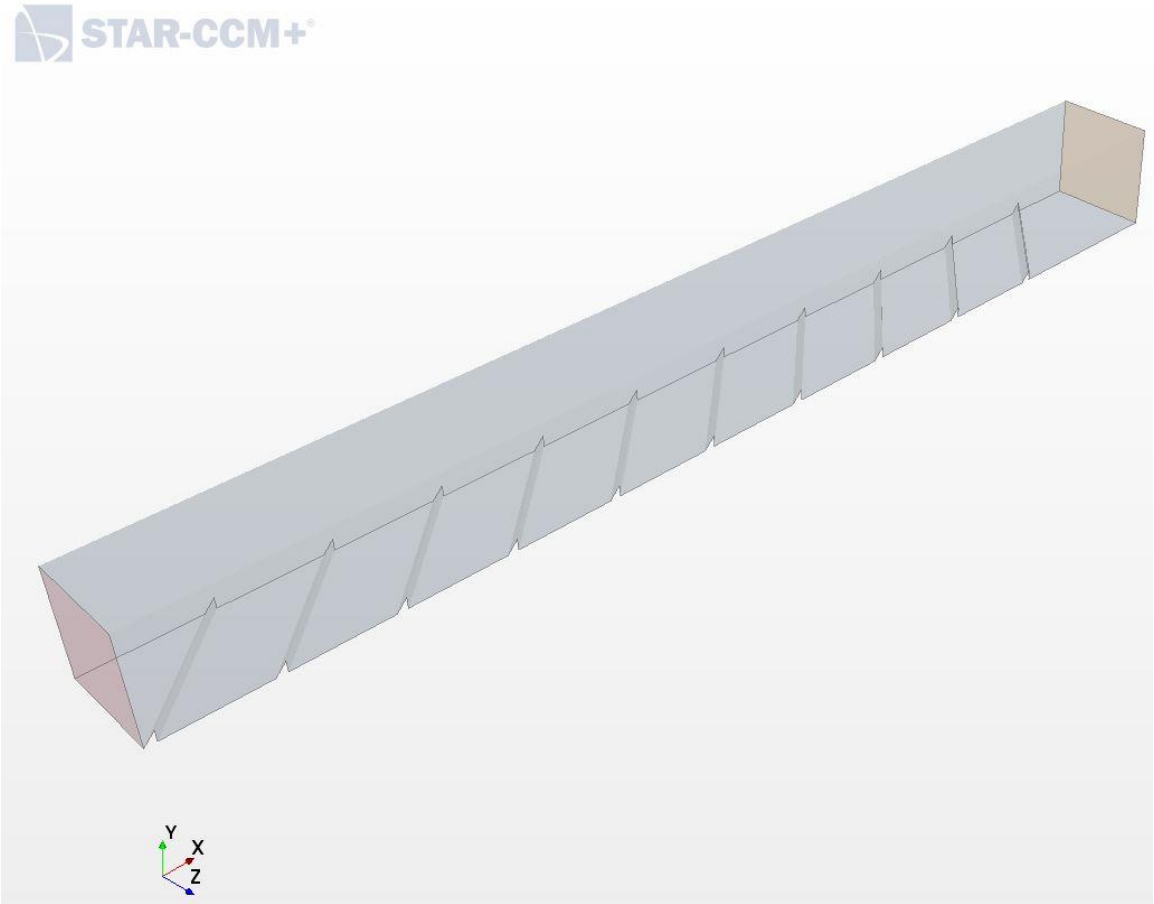

Figure 4.42. CAD model of 45° right triangular rib pointing upstream

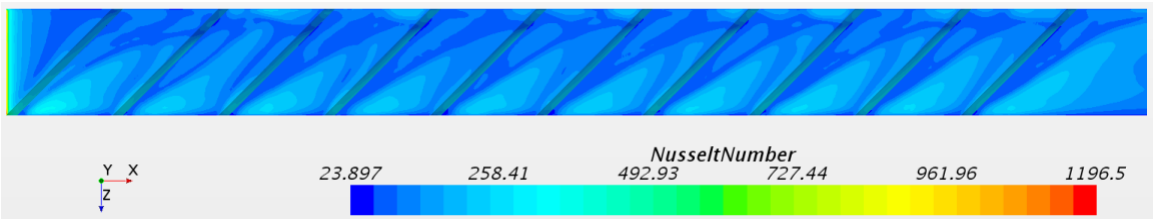

Figure 4.43. Nusselt number contour plot for 45° right triangular rib pointing upstream

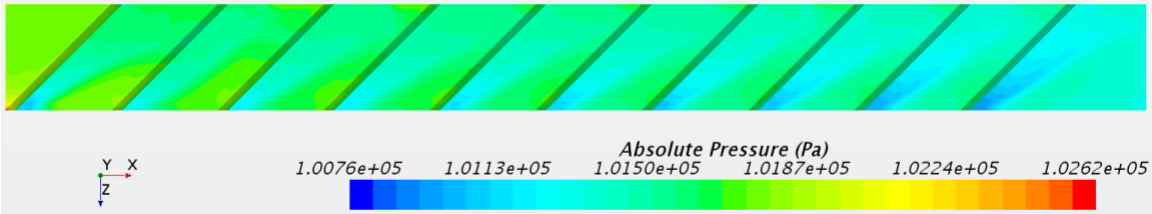

Figure 4.44. Absolute Pressure contour plot for 45° right triangular rib pointing upstream

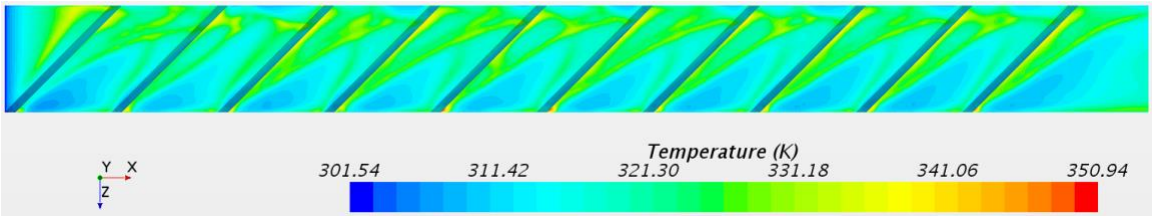

Figure 4.45. Temperature contour plot for 45° right triangular rib pointing upstream

4.7 Pie-Slice Rib Pointing Downstream Results

4.7.1 Transverse Pie-Slice Rib Pointing Downstream Results

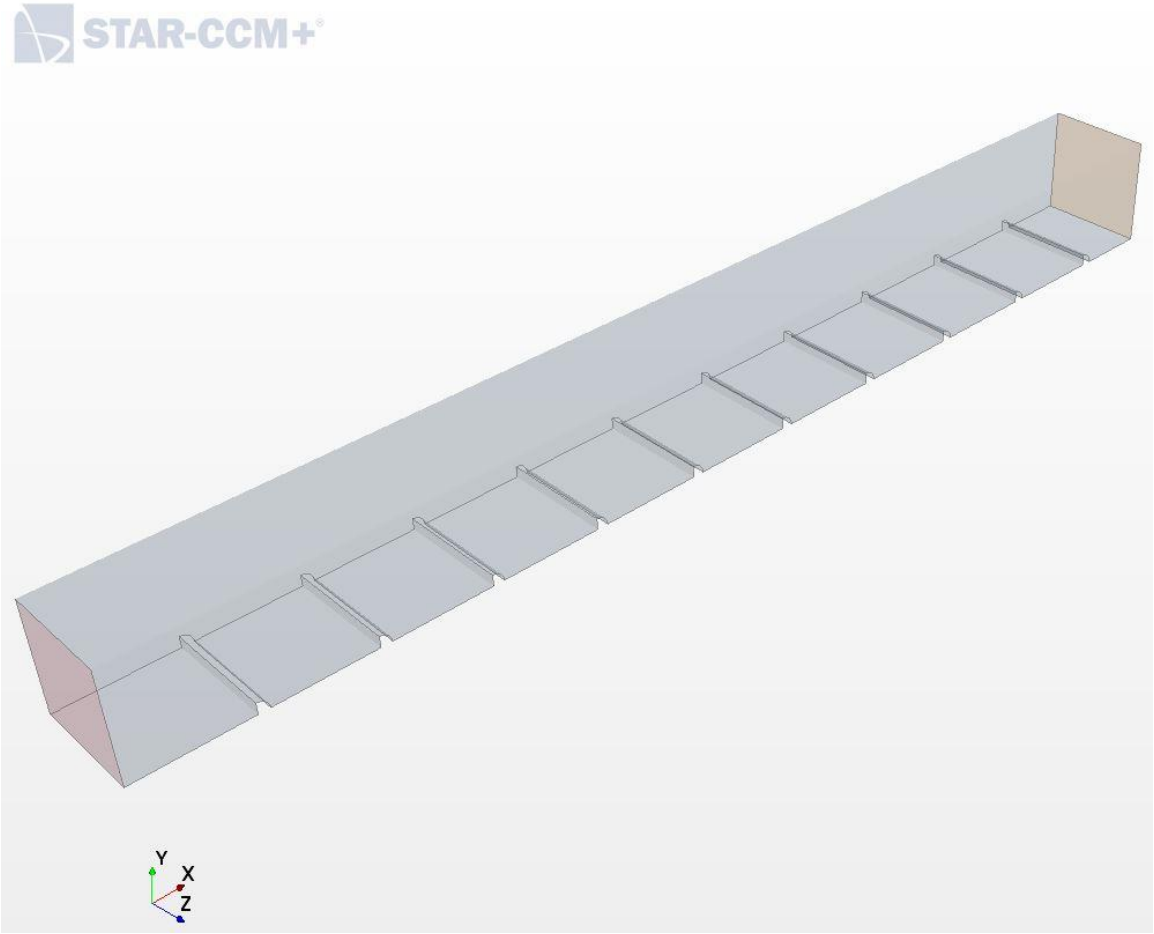

Figure 4.46. CAD model of transverse pie-slice rib pointing downstream

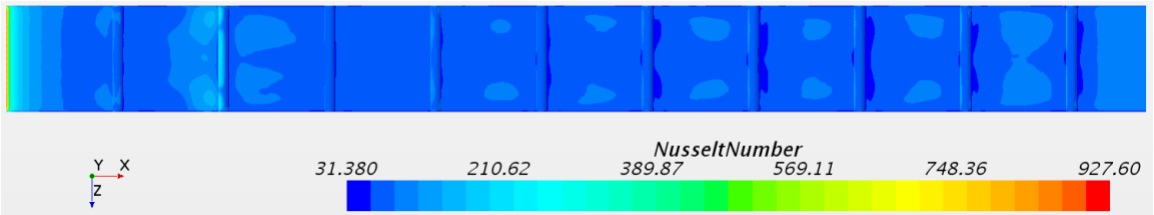

Figure 4.47. Nusselt number contour plot for transverse pie-slice rib pointing downstream

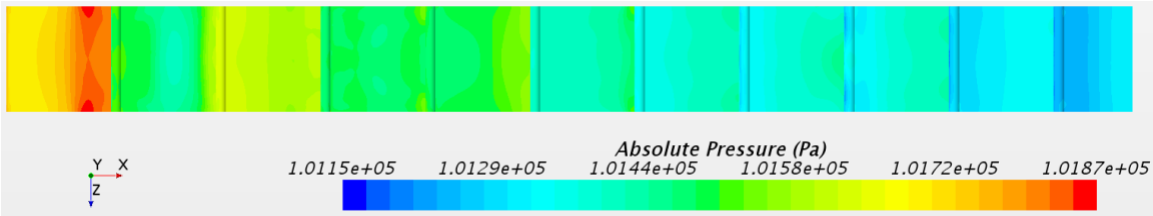

Figure 4.48. Absolute Pressure contour plot for transverse pie-slice rib pointing downstream

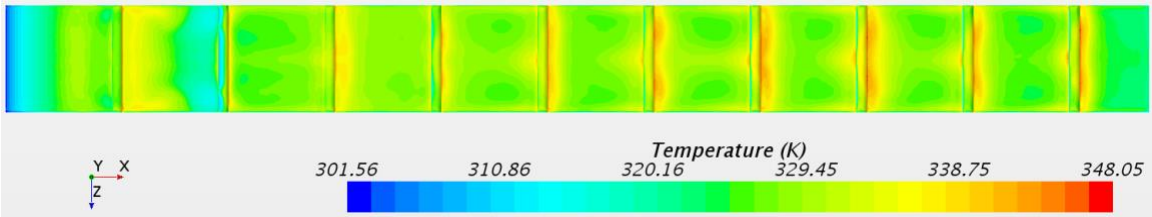

Figure 4.49. Temperature contour plot for transverse pie-slice rib pointing downstream

4.7.2 45° Pie-Slice Rib Pointing Downstream Results

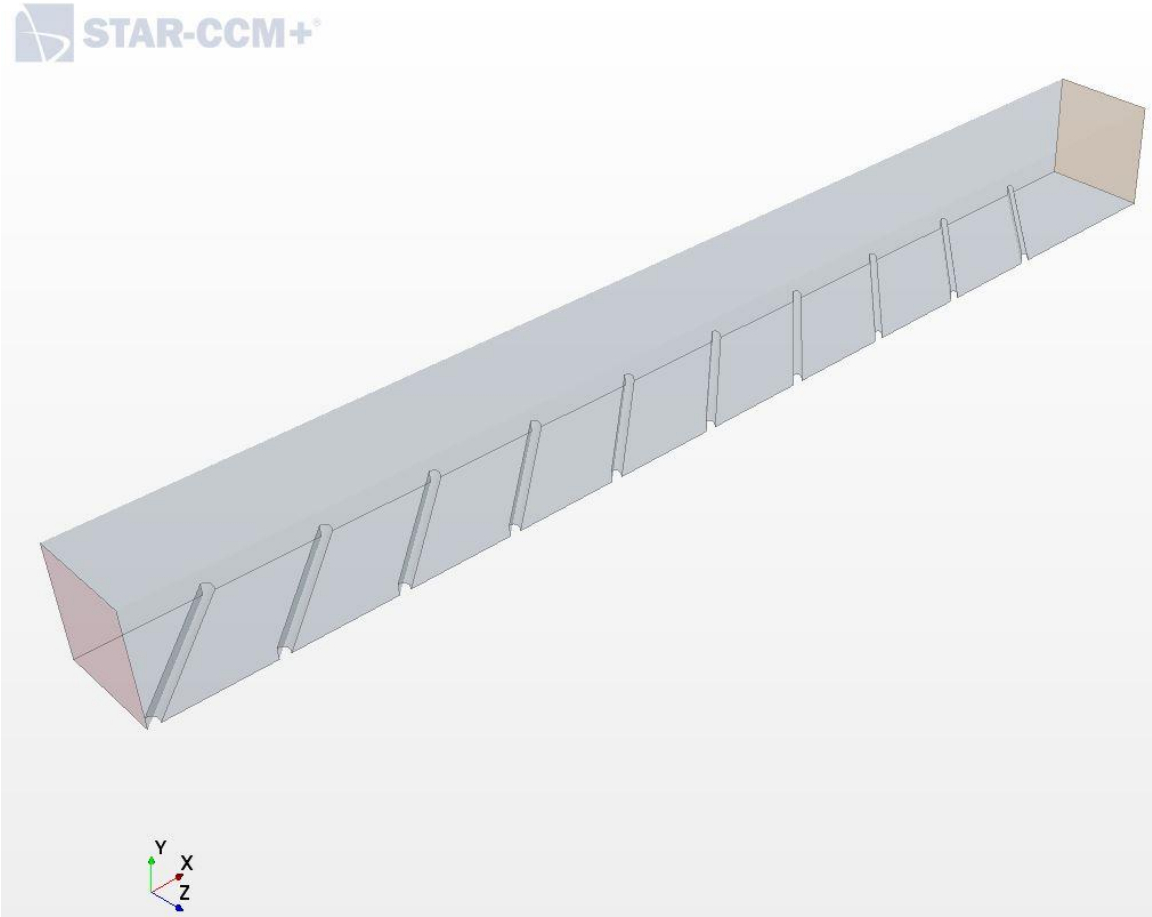

Figure 4.50. CAD model of 45° pie-slice rib pointing downstream

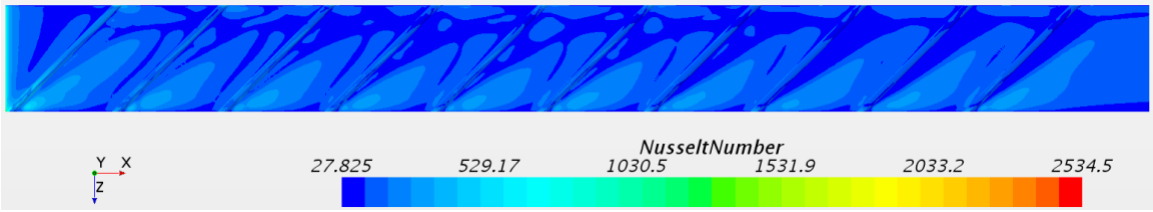

Figure 4.51. Nusselt number contour plot for 45° pie-slice rib pointing downstream

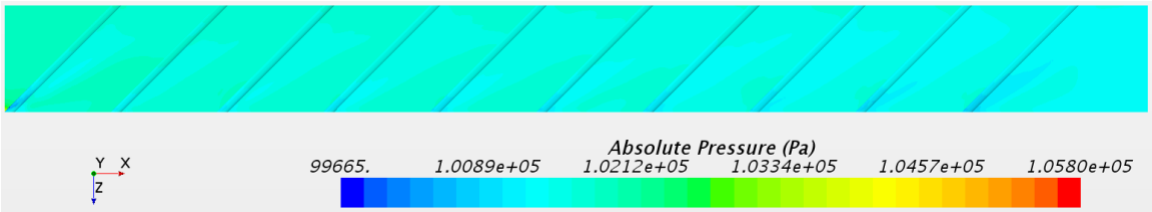

Figure 4.52. Absolute Pressure contour plot for 45° pie-slice rib pointing downstream

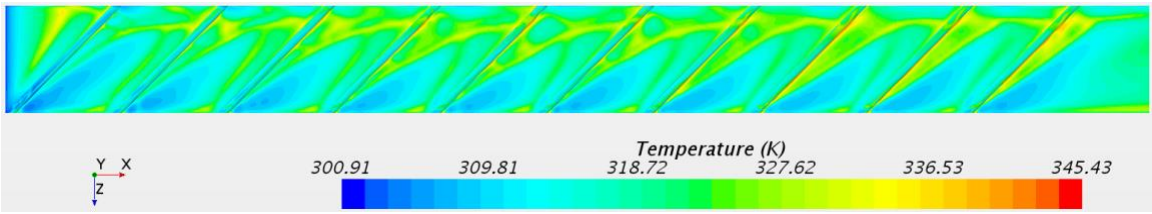

Figure 4.53. Temperature contour plot for 45° pie-slice rib pointing downstream

4.8 Pie-Slice Rib Pointing Upstream Results

4.8.1 Transverse Pie-Slice Rib Pointing Upstream Results

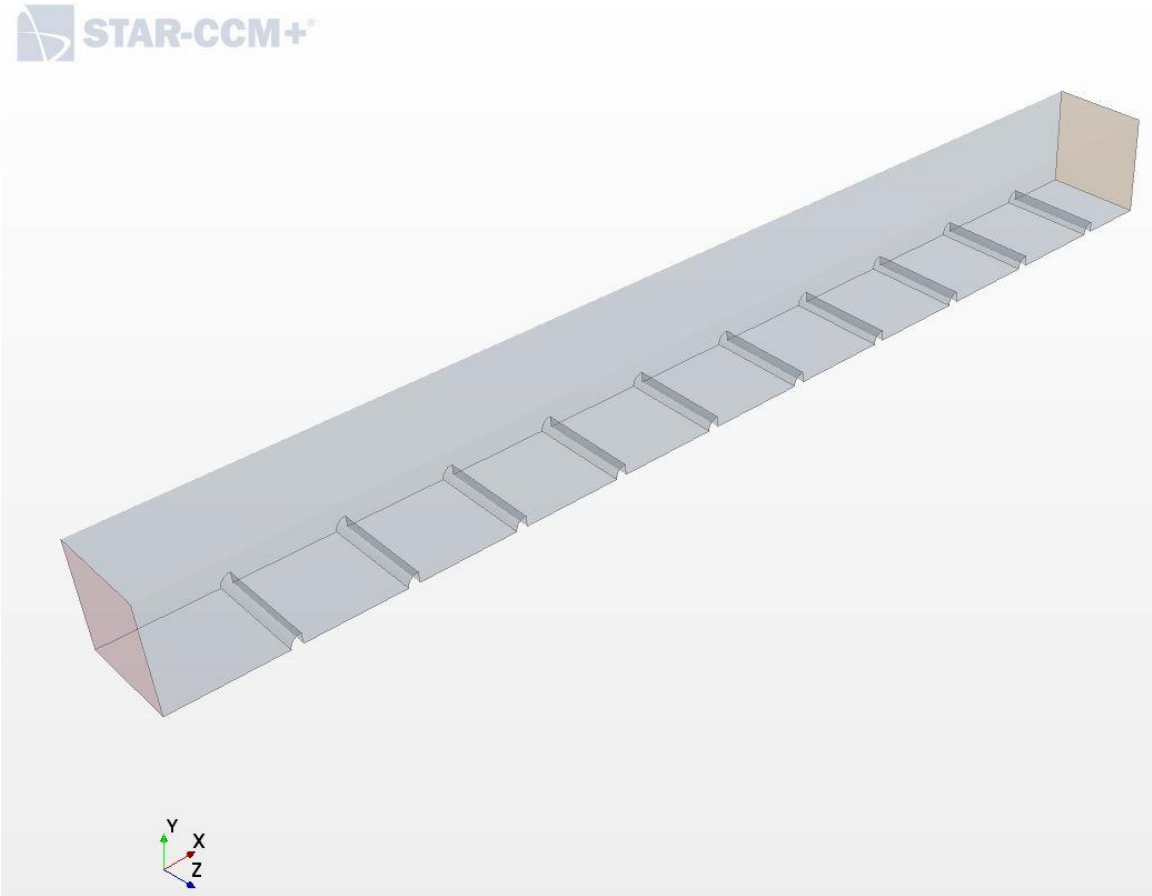

Figure 4.54. CAD model of transverse pie-slice rib pointing upstream

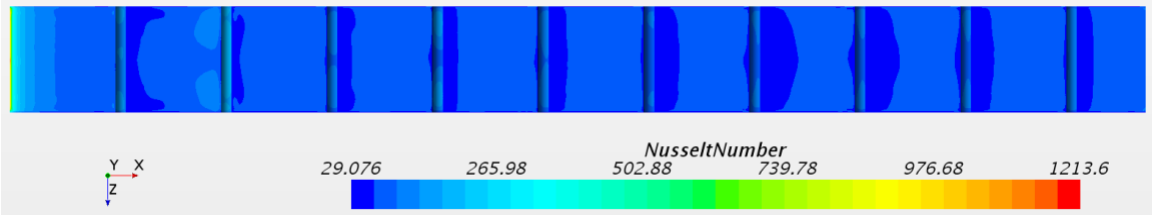

Figure 4.55. Nusselt number contour plot for transverse pie-slice rib pointing upstream

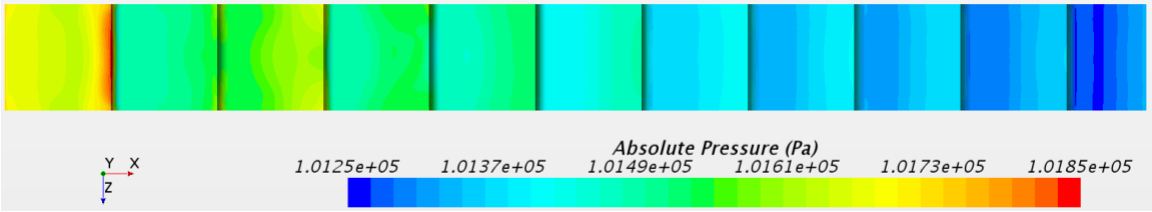

Figure 4.56. Absolute Pressure contour plot for transverse pie-slice rib pointing upstream

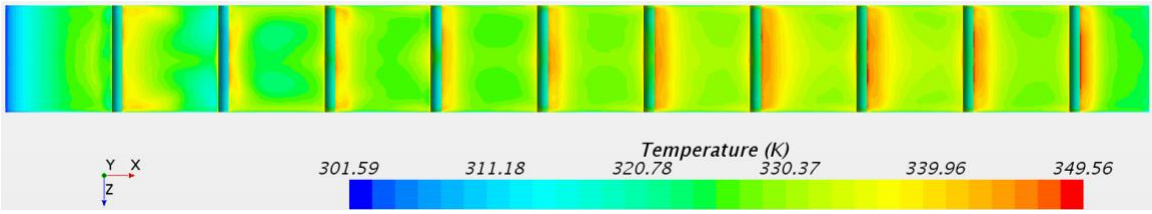

Figure 4.57. Temperature contour plot for transverse pie-slice rib pointing upstream

4.8.2 45° Pie-Slice Rib Pointing Upstream Results

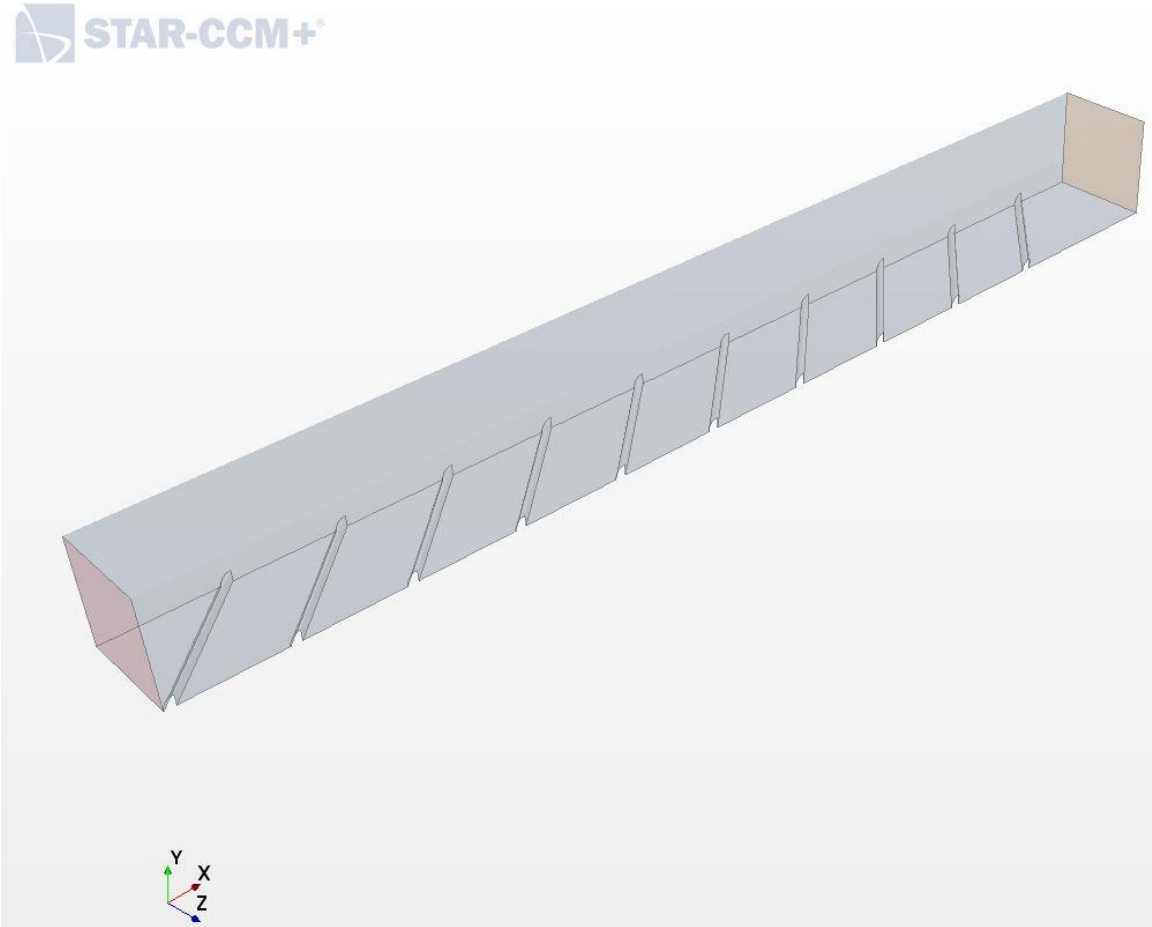

Figure 4.58. CAD model of 45° pie-slice rib pointing upstream

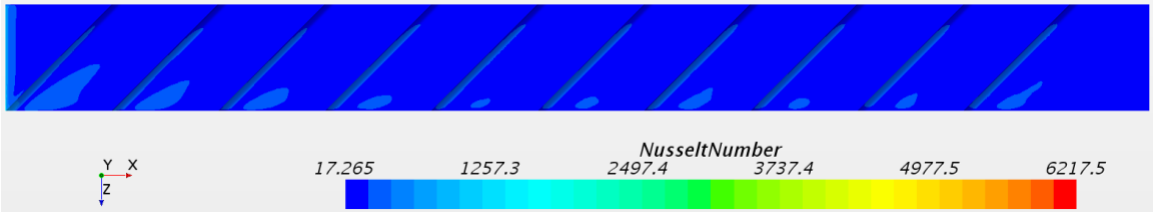

Figure 4.59. Nusselt number contour plot for 45° pie-slice rib pointing upstream

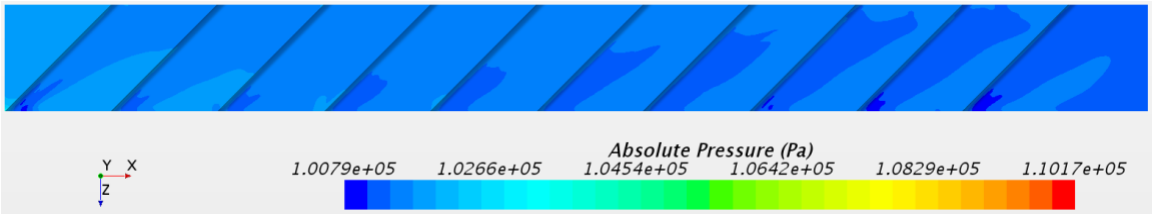

Figure 4.60. Absolute Pressure contour plot for 45° pie-slice rib pointing upstream

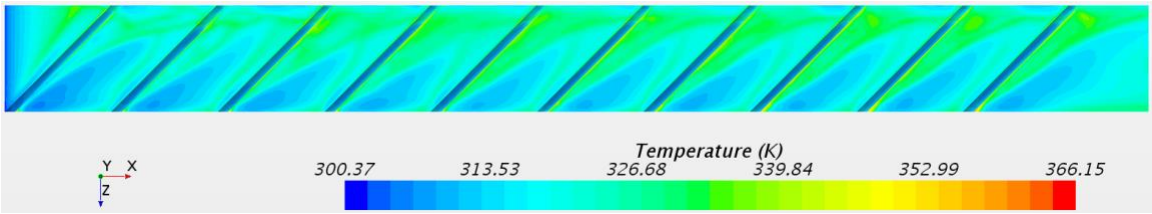

Figure 4.61. Temperature contour plot for 45° pie-slice rib pointing upstream

4.9 Rectangular Rib Results

4.9.1 Transverse Rectangular Rib Results

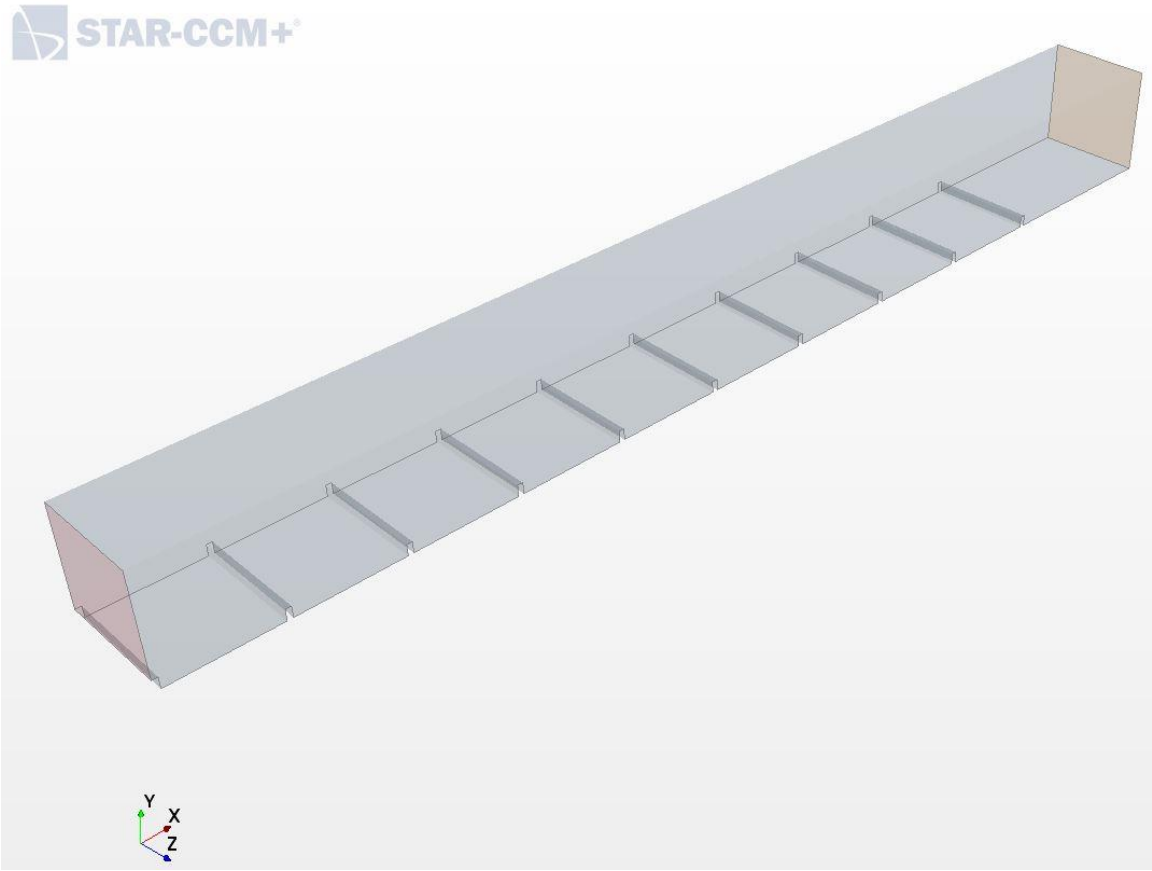

Figure 4.62. CAD model of transverse rectangular rib

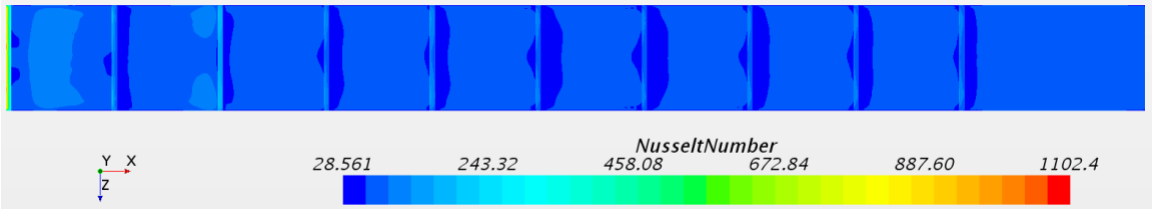

Figure 4.63. Nusselt number contour plot for transverse rectangular rib

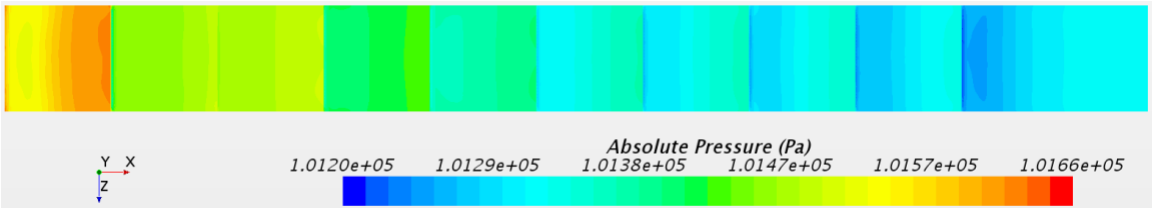

Figure 4.64. Absolute Pressure contour plot for transverse rectangular rib

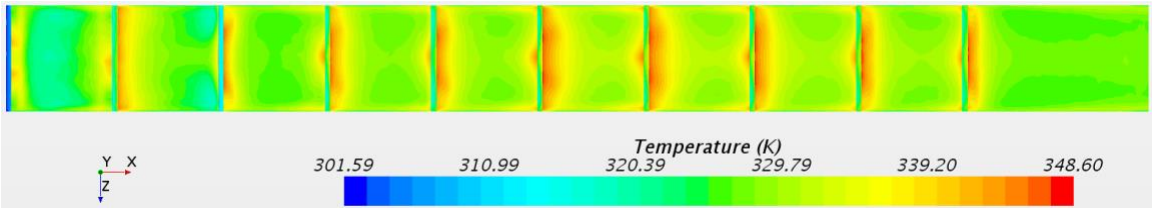

Figure 4.65. Temperature contour plot for transverse rectangular rib

4.9.2 45° Rectangular Rib Results

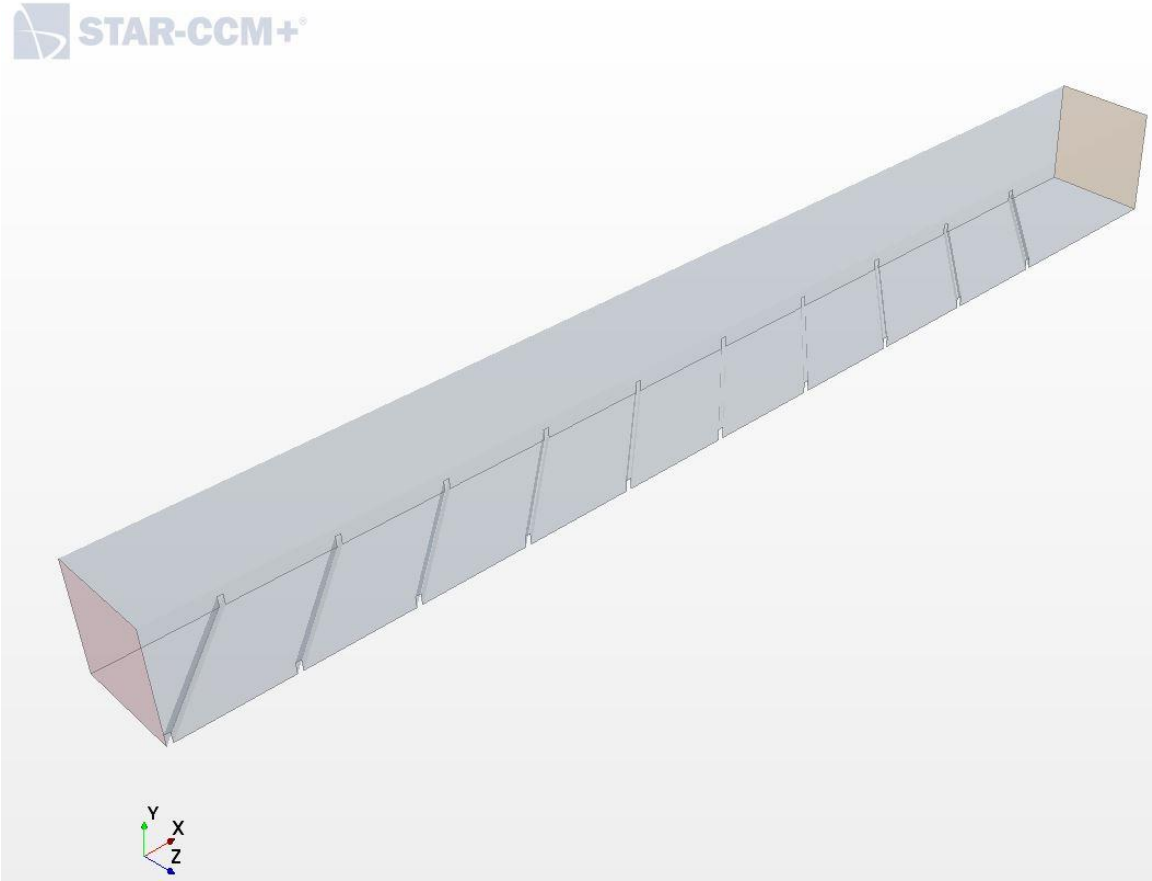

Figure 4.66. CAD model of 45° rectangular rib

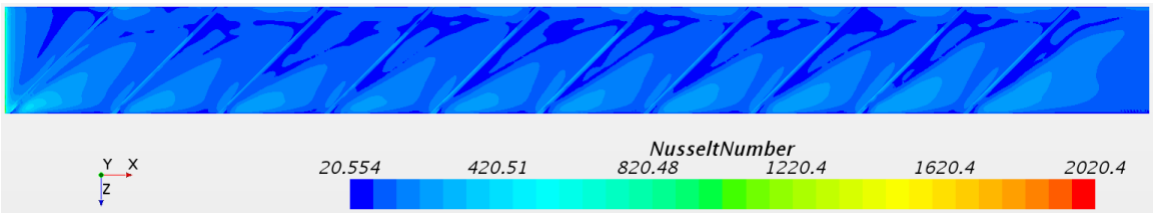

Figure 4.67. Nusselt number contour plot for 45° rectangular rib

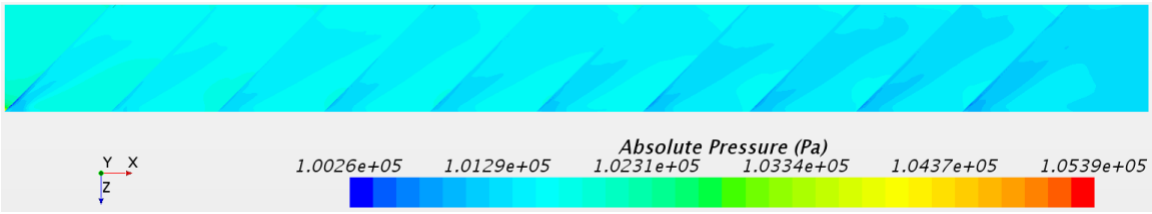

Figure 4.68. Absolute Pressure contour plot for 45° rectangular rib

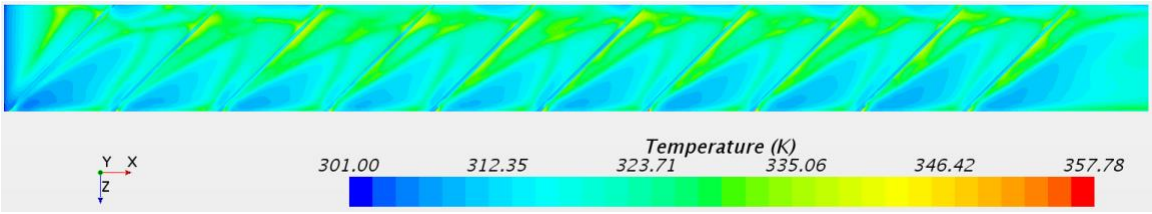

Figure 4.69. Temperature contour plot for 45° rectangular rib

4.10 Comparison of Transverse Ribs

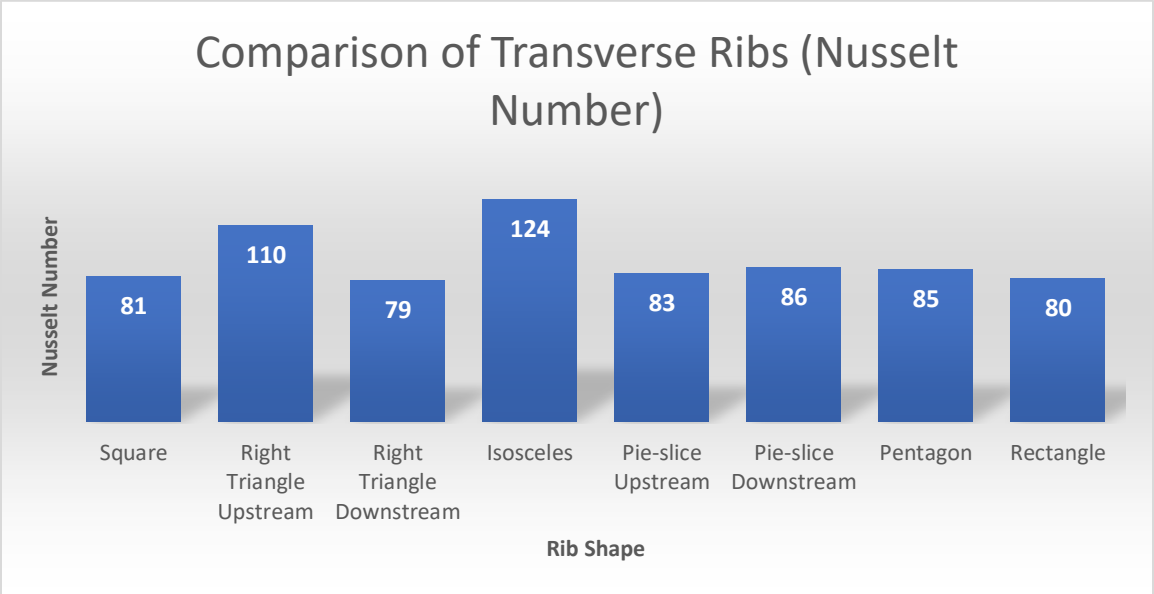

Figure 4.70. Average Nusselt number of rib-roughened surface of different rib shapes (transverse)

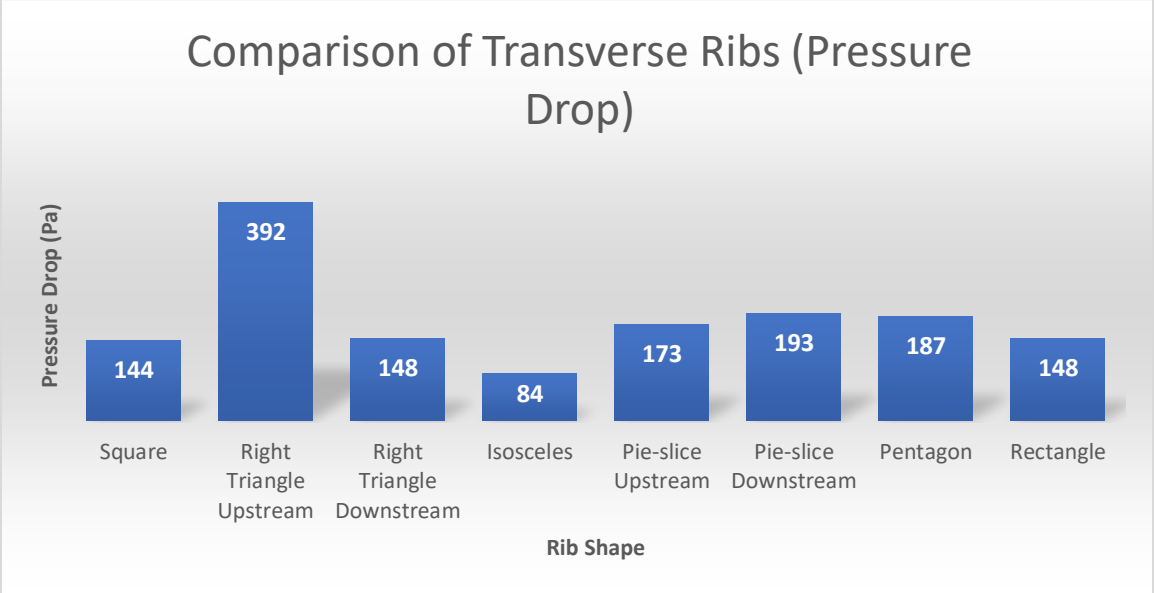

Figure 4.71. Pressure drop between inlet and outlet of square channel of different rib shapes (transverse)

4.11 Comparison of 45° Ribs

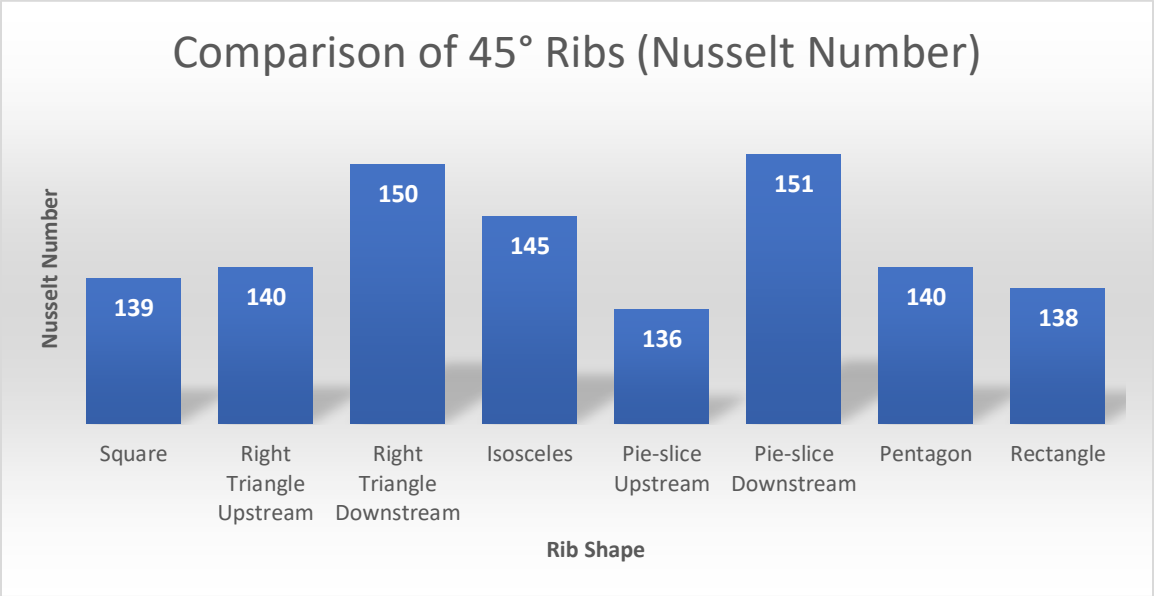

Figure 4.72. Average Nusselt number of rib-roughened surface of different rib shapes (45°)

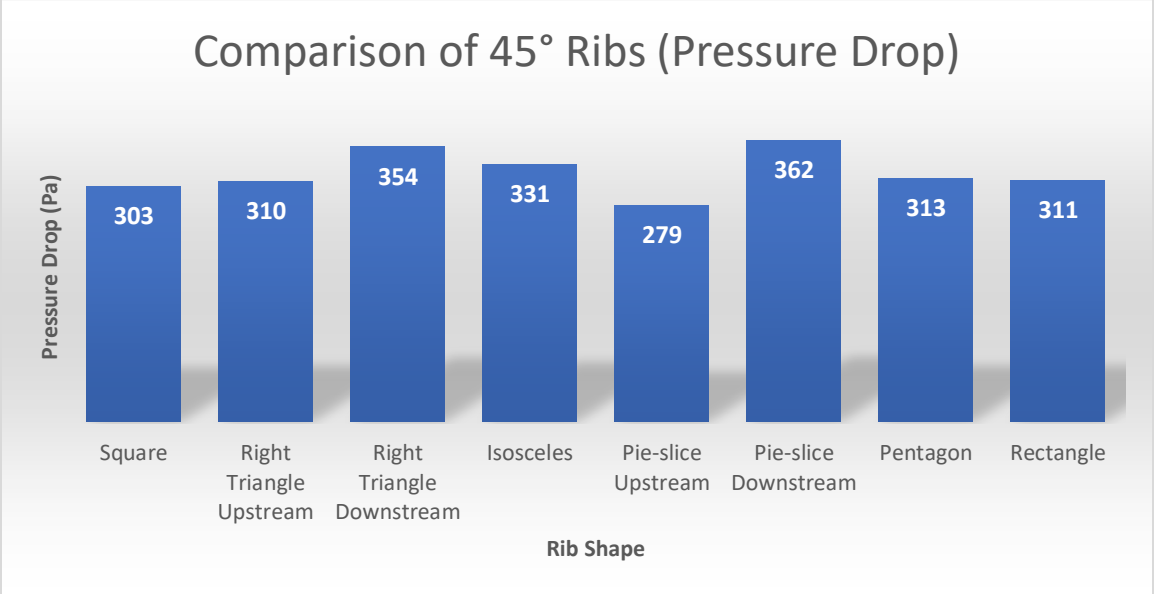

Figure 4.73. Pressure drop between inlet and outlet of square channel of different rib shapes (45°)

4.12 Comparison of Transverse and 45° Ribs

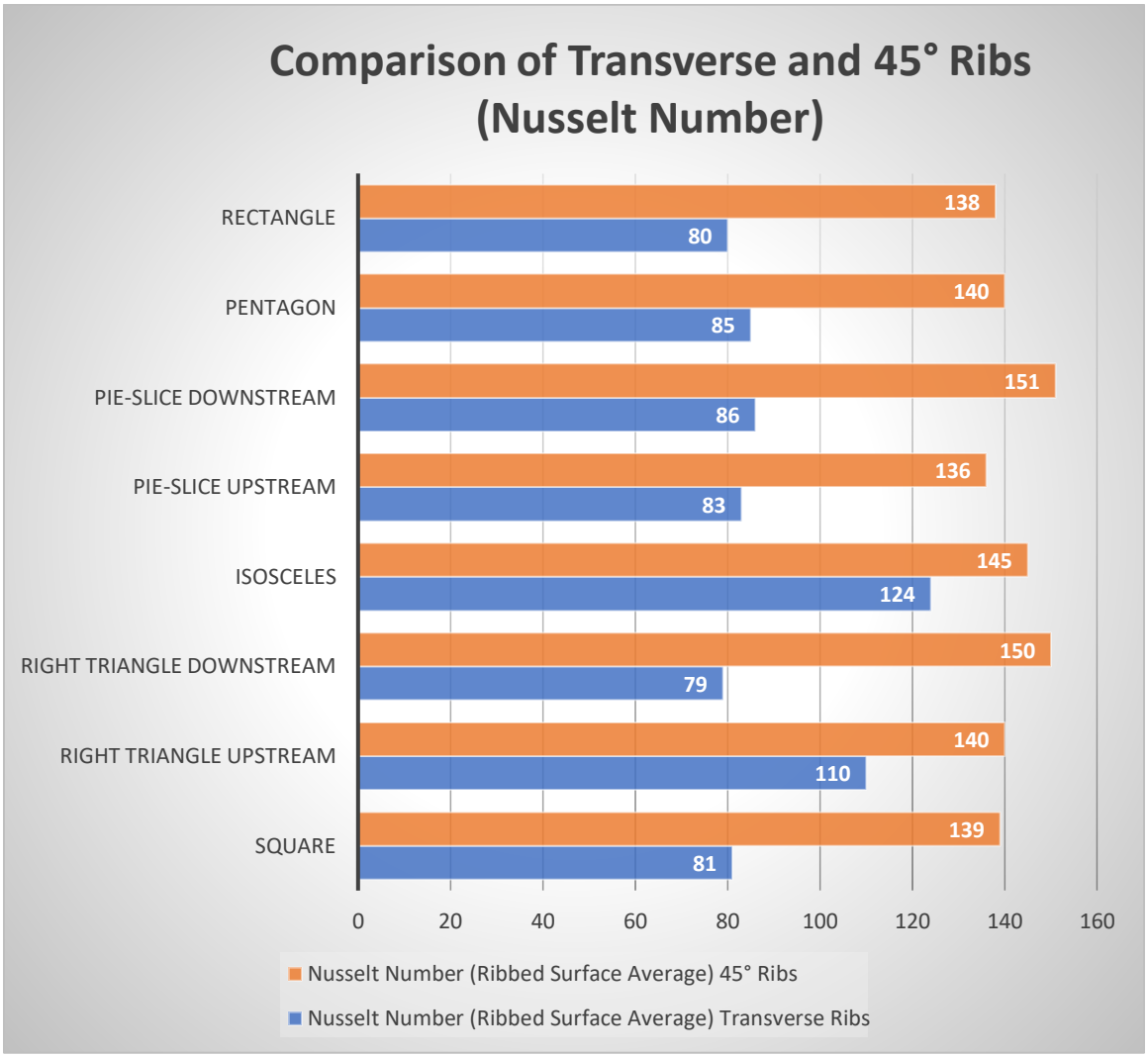

Figure 4.74. Average Nusselt number of the rib-roughened surface of transverse and 45° ribs

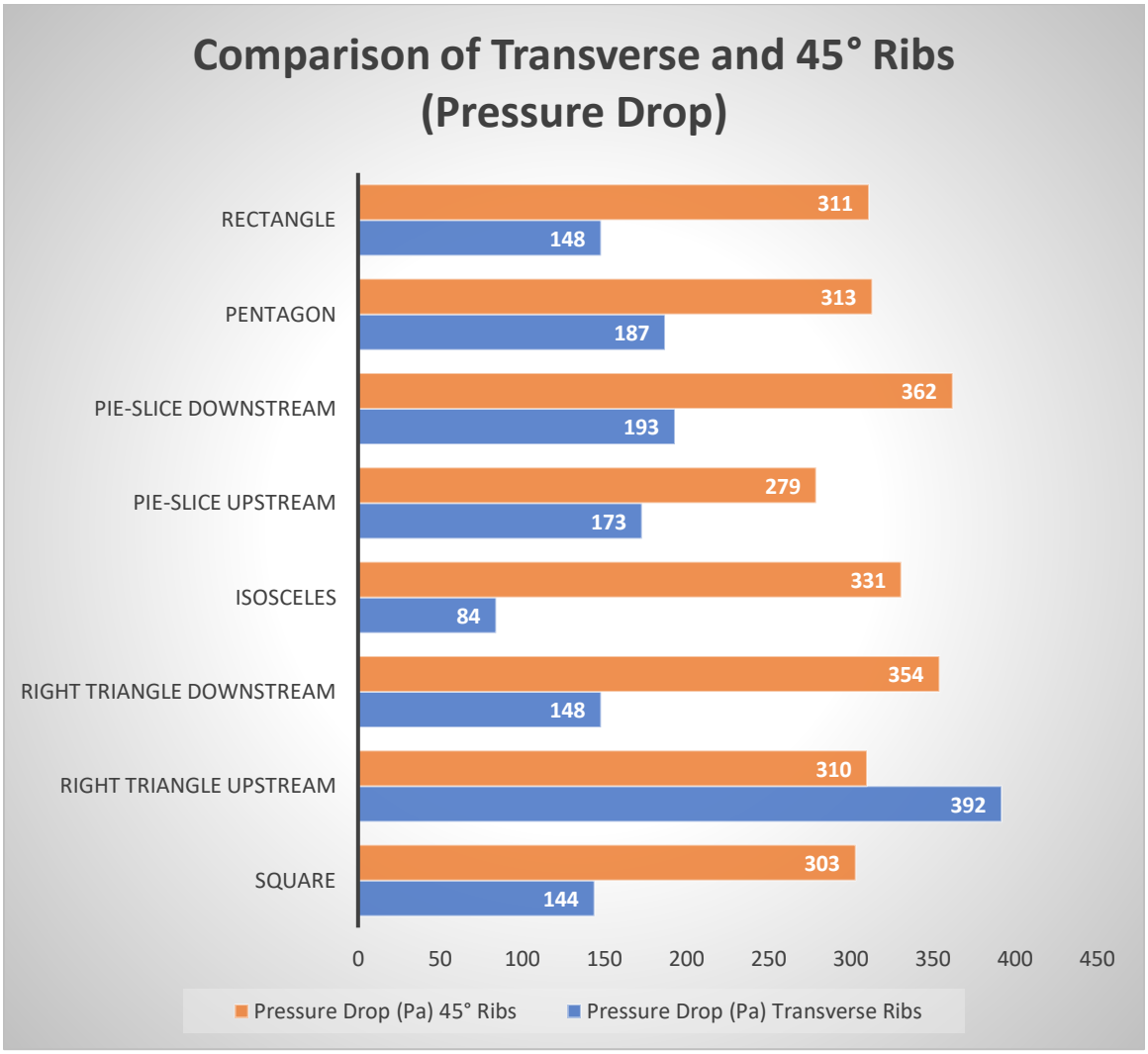

Figure 4.75. Pressure drop between inlet and outlet of square channel of transverse and 45° ribs

CHAPTER 5: CONCLUSION

The RANS simulations were run to analyze the heat transfer characteristics and pressure drop with different shapes of ribs. The important observations are summarized below:

- For transverse ribs, the Nusselt number varied the most with the change of shape of ribs. Isosceles triangular ribs had the highest average Nusselt number of Rib-roughened surface and right triangular ribs pointing upstream had the highest pressure drop between inlet and outlet.
- For 45° angled ribs, pie-slice shaped ribs pointing downstream had the highest average Nusselt number and pressure drop.
- Average Nusselt number and pressure drop were higher for 45° ribs compared to transverse ribs in all shapes of ribs except right triangular ribs pointing upstream (pressure drop).

CHAPTER 6: FUTURE WORK

The heat transfer performance of the existing models can be improved and understood better. Some suggestions for future work are given below:

- Determine the optimum pitch-to-height ratio for a specific shape of rib.
- Run CFD simulations with more complicated rib shapes.
- Run CFD simulations with inline and staggered ribs on opposite walls of the channel with different shapes of rib.
- Run LES simulations to replicate the unsteady nature of the flow in the experiments.

APPENDIX

Procedure for running channel flow CFD simulation in STARCCM+:

- Generate CAD model
    - Open STARCCM+
    - Click on new simulation on top left or go to File>New
    - Select Serial or Parallel on Local Host and click OK
    - Expand Geometry and Right click on 3D-CAD Models and Select New
    - Right click on ZX-plane under Features and select Create Sketch
    - Click on View Normal to Sketch Plane
    - Select Create Line to draw the base for the channel and click OK
    - Right click on Sketch 1, select Create Extrude and type required value for Distance, click OK to produce the three-dimensional representation of the channel
    - Right click on the face of three-dimensional body and select Create Plane by Transformation and click OK.
    - Right click on Plane 1 and select Create Sketch
    - Click on View Normal to Sketch Plane
    - Draw the outline of the shape of rib
    - Right click on Sketch 2 and select Create Extrude Cut and click OK
    - Right click on the faces and Rename Boundaries: Inlet, Outlet, Top, Left, Right, Ribbed-Surface (Bottom) and click on Close 3D-CAD.
    - Right click on 3D-CAD Model 1 and select New Geometry Part and click OK on Part Creation Option dialogue box

- Expand Parts and right click on Body 1, select Assign Parts to Regions
- Select Create a Region for Each Part and Create a Boundary for Each Part Surface in the first two dropdown menu of Assign Parts to Regions dialogue box and click Apply and Close.

- Generate Mesh
  - Right click on Continua, expand New and select Mesh Continuum
  - Right click on Models under Mesh 1 and choose Select Meshing Models
  - Check on:
    1. Surface Remesher,
    2. Surface Wrapper,
    3. Advancing Layer Mesher,
    4. Extruder and click Close.
  - Expand Reference Values and modify variables as needed
  - Custom mesh may be required depending on geometry
  - Click on the cube icon in the top menu bar
- Select Physics Models
  - Expand Physics 1 under Continua, right click on models and choose Select models
  - Check on:
    1. Three Dimensional
    2. Steady
    3. Gas
    4. Coupled Flow

5. Ideal Gas
6. Turbulent
7. *K*-Omega Turbulence and click Close.

- Define Boundary Conditions
  - Expand Regions > Body 1 > Boundaries, and right click on them individually and select Edit
  - In the dialogue box select appropriate boundary conditions under Type dropdown menu:
    1. Inlet (Velocity Inlet)
    2. Outlet (Pressure Outlet)
    3. Top (Wall)
    4. Left (Wall)
    5. Right (Wall)
    6. Ribbed-Surface (Wall)
- Change Default Variables
  - Expand Inlet, Physics Values and click on Velocity Magnitude and change the value as required
  - Expand Ribbed-Surface, Physics conditions, click on Thermal Specification and in Properties choose Heat Flux
  - Expand Physics Values under Ribbed-Surface, click on Heat Flux and change Value field as required
- Prepare Visualization for Results
  - Right click on Scenes > New Scene > Scalar

  - Go to Scenes > Scalar Scene 1 > Displayers and select required parameter from Scalar 1 > Scalar Field and required plane/surface from Scalar 1 > Parts.
  - Go to Tools > Field Functions and select required parameter and change properties depending on geometry and physics.
- Prepare Reports for Result Analysis
  - Right click on Report > New Report and select appropriate variable
  - Select plane/surface for Parts and parameter for Field Function in Properties
- Run Simulation
  - Click on Initialize Solution (green flag symbol on menu bar) or go to Solution tab and click on Initialize Solution
  - Click Run (a running human symbol) or press CTRL+R on keyboard

REFERENCES

[1] J.-C. Han, S. Dutta, and S. Ekkad, *Gas turbine heat transfer and cooling technology*. CRC Press, 2012.

[2] R. J. Goldstein, "Film cooling," in *Advances in heat transfer*, vol. 7: Elsevier, 1971, pp. 321-379.

[3] J.-C. Han and S. Ekkad, "Recent development in turbine blade film cooling," *International Journal of Rotating Machinery,* vol. 7, no. 1, pp. 21-40, 2001.

[4] S. Farokhi, *Aircraft propulsion*. John Wiley & Sons, 2014.

[5] J. Han, J. S. Park, and C. Lei, "Heat transfer and pressure drop in blade cooling channels with turbulence promoters," 1984.

[6] D. Singh and J. J. Doom, "Simulations of impinging jets with a range of configuration," in *55th AIAA Aerospace Sciences Meeting*, 2017, p. 0751.

[7] B. Lakshminarayana, *Fluid dynamics and heat transfer of turbomachinery*. John Wiley & Sons, 1995.

[8] J. Han and S. Dutta, "Internal convection heat transfer and cooling: An experimental approach," *Lecture series-van Kareman Institute for fluid dynamics*, vol. 5, pp. C1-C147, 1995.

[9] J. Han, J. S. Park, and C. Lei, "Heat transfer enhancement in channels with turbulence promoters," *Journal of Engineering for Gas Turbines and Power,* vol. 107, no. 3, pp. 628-635, 1985.

[10] J. Han and J. S. Park, "Developing heat transfer in rectangular channels with rib turbulators," *International Journal of Heat and Mass Transfer,* vol. 31, no. 1, pp. 183-195, 1988.

[11] W. Peng, P.-X. Jiang, Y.-P. Wang, and B.-Y. Wei, "Experimental and numerical investigation of convection heat transfer in channels with different types of ribs," *Applied Thermal Engineering*, vol. 31, no. 14-15, pp. 2702-2708, 2011.

[12] M. Taslim, T. Li, and D. Kercher, "Experimental heat transfer and friction in channels roughened with angled, V-shaped and discrete ribs on two opposite walls," in *ASME 1994 International Gas Turbine and Aeroengine Congress and Exposition*, 1994, pp. V004T09A018-V004T09A018: American Society of Mechanical Engineers.

[13] R. Kiml, S. Mochizuki, and A. Murata, "Effects of rib arrangements on heat transfer and flow behavior in a rectangular rib-roughened passage: application to cooling of gas turbine blade trailing edge," *Journal of heat transfer*, vol. 123, no. 4, pp. 675-681, 2001.

[14] M. E. Taslim and S. D. Spring, "Effects of turbulator profile and spacing on heat transfer and friction in a channel," *Journal of Thermophysics and Heat Transfer*, vol. 8, no. 3, pp. 555-562, 1994.

[15] J. Ahn and J. S. Lee, "Large eddy simulation of flow and heat transfer in a channel with a detached rib array," *International Journal of Heat and Mass Transfer*, vol. 53, no. 1-3, pp. 445-452, 2010.

[16] T. Chompookham, C. Thianpong, S. Kwankaomeng, and P. Promvonge, "Heat transfer augmentation in a wedge-ribbed channel using winglet vortex generators," *International Communications in Heat and Mass Transfer*, vol. 37, no. 2, pp. 163-169, 2010.

[17] P. Promvonge, T. Chompookham, S. Kwankaomeng, and C. Thianpong, "Enhanced heat transfer in a triangular ribbed channel with longitudinal vortex generators," *Energy Conversion and Management,* vol. 51, no. 6, pp. 1242-1249, 2010.

[18] S. Sripattanapipat and P. Promvonge, "Numerical analysis of laminar heat transfer in a channel with diamond-shaped baffles," *International Communications in Heat and Mass Transfer,* vol. 36, no. 1, pp. 32-38, 2009.

[19] G. Rau, M. Cakan, D. Moeller, and T. Arts, "The effect of periodic ribs on the local aerodynamic and heat transfer performance of a straight cooling channel," in *ASME 1996 International Gas Turbine and Aeroengine Congress and Exhibition*, 1996, pp. V004T09A061-V004T09A061: American Society of Mechanical Engineers.

[20] C. Nonino and G. Comini, "Convective heat transfer in ribbed square channels," *International Journal of Numerical Methods for Heat & Fluid Flow,* vol. 12, no. 5, pp. 610-628, 2002.

[21] S. W. Ahn, H. K. Kang, S. T. Bae, and D. H. Lee, "Heat transfer and friction factor in a square channel with one, two, or four inclined ribbed walls," *Journal of Turbomachinery*, vol. 130, no. 3, p. 034501, 2008.

[22] F. Shin, Y. Wen-Jei, and Z. Nengli, "Local heat transfer in a rotating serpentine passage with rib-roughened surfaces," *International Journal of Heat and Mass Transfer,* vol. 37, no. 2, pp. 217-228, 1994.

[23] W.-L. Fu, L. M. Wright, and J.-C. Han, "Heat transfer in two-pass rotating rectangular channels (AR = 2: 1) with discrete ribs," *Journal of thermophysics and heat transfer,* vol. 20, no. 3, pp. 569-582, 2006.

[24] S. V. Ekkad, G. Pamula, and M. Shantiniketanam, "Detailed heat transfer measurements inside straight and tapered two-pass channels with rib turbulators," *Experimental Thermal and Fluid Science,* vol. 22, no. 3-4, pp. 155-163, 2000.

[25] L. Wang and B. Sundén, "Experimental investigation of local heat transfer in a square duct with various-shaped ribs," *Heat and Mass Transfer,* vol. 43, no. 8, p. 759, 2007.

[26] S. W. Chang and Z.-X. Cai, "Heat transfer and pressure drop in two-pass rib-roughened square channels with bleed from sharp bend," *International Journal of Heat and Fluid Flow,* vol. 31, no. 1, pp. 19-31, 2010.